

Article

# Integrating Remote Sensing and Hydrologic Modeling to Assess the Impact of Land-Use Changes on the Increase of Flood Risk: A Case Study of the Riyadh–Dammam Train Track, Saudi Arabia

Ashraf Abdelkarim <sup>1,\*</sup> , Ahmed F. D. Gaber <sup>2,3</sup> , Ibtesam I. Alkadi <sup>4</sup> and Haya M. Alogayell <sup>4</sup><sup>1</sup> Research Center, Ministry of Housing, Riyadh 11461, Saudi Arabia<sup>2</sup> Department of Geography, Faculty of Art, Sohag University, Sohag 82524, Egypt; adahy70@gmail.com<sup>3</sup> Geography and GIS Department, College of Arts, Imam Abdulrahman Bin Faisal University, Dammam 31441, Saudi Arabia<sup>4</sup> Geography Department, College of Arts, Princess Nourah bint Abdulrahman University, Riyadh 84428, Saudi Arabia; Ebtesam.K@gmail.Com (I.I.A.); hayaalogayell@gmail.com (H.M.A.)

\* Correspondence: dr.ashrafgis2020@gmail.com

Received: 12 September 2019; Accepted: 24 October 2019; Published: 28 October 2019



**Abstract:** The current study aimed at measuring the impact of the change in land-use morphology on the increase of flood risk through its application to the case of the Riyadh–Dammam train track in Saudi Arabia. The track was exposed to drift on 18 February 2017, over a length of 10 km, in the district of Dhahran in the capital of Dammam. Flooding caused the train to drift off its track and resulted in damage to lives, property, and infrastructure. This resulted from human interventions in the preplanning land uses and changing the morphology of the land by encroaching on the valleys, which resulted in the loss of the environmental and ecological balance in the study area. In order to achieve these goals, land-use changes in the study area were monitored by analyzing successive images from the GEO-I-1 satellite with a resolution of 60 cm for the years 2011 and 2017, before and after the train drift, using the maximum likelihood classification process provided in ERDAS IMAGINE 2016. GIS was used in the processing of 1 m digital elevation models to extract the morphological changes of the wadies between 2011 and 2017. A hydrological model (HEC–HMS) was used in calculating the (flood) hydrograph curve of the wadies basins and estimating the calculation of flood water quantities and its flow rates based on the Soil Conservation Services (SCS) Unit Hydrograph Method. Rain depth was analyzed and estimated for different return periods. The HEC–RAS hydraulic modeling program was employed in developing a 2D model to calculate the velocity, depth, and spread of the flood in order to apply the risk matrix method.

**Keywords:** land-use changes; wadi morphology; flood risk; Riyadh–Dammam train track; hydrological and hydraulic modeling; sustainable development

## 1. Introduction

Land-use changes play an important role in the hydrological behavior of drainage basins and affect the local hydrological cycle. Several studies have been conducted to assess the impact of land-use changes on runoff [1–5]. Land use and land cover changes are affected by attempts to meet human needs such as in the construction of residential, industrial, and agricultural facilities, mining, as well as other infrastructure facilities that are key processes associated with economic and sustainable growth of the area [6]. The proper use of available land is essential for improving the economic and planning status of the area without expanding to areas prone to risk, which is an essential issue

for sustainable planning [6,7]. Urban flooding has been, and continues to be, a major problem for many cities throughout the developed and developing world. The need to formulate a sound flood management policy driven by knowledge of the frequency and magnitude of these floods is essential to improve the impacts of these floods. Flood risk maps can be used by design engineers as an effective tool for water resources and urban planning to assess the vulnerability of the infrastructure and residents of that area to flood events [8].

The record of flood events registered between 1950 and 2017 indicates that most floods have occurred in recent decades. About 2% of floods occurred during the 1950s and increased rapidly every decade thereafter to about 3.9%, 6.6%, 13.2%, 21.9%, and 52.2% for the sixties, seventies, eighties, nineties, and the millennium, respectively. Floods accounted for more than two-thirds of the hydrological disasters during the period from 2012 to 2014 and reached 90.9% during the period from 2015 to 2016. More than 60% of total economic and human losses took place during the period from 1950 to 2016 in Asia. In Saudi Arabia, floods were characterized as one of the most frequent and devastating natural disasters [9].

Many authors acknowledged the fact that increased urban activities in flood areas will increase peak discharge, reduce peak time, and increase surface runoff [10–14]. A better understanding and assessment of land-use changes that have a direct impact on watershed hydrological processes is critical to the planning, management, and sustainable development of watersheds [15–18]. Recently, geomatics of remote sensing (RS) and geographic information systems (GIS) have been employed as powerful and effective tools for determining land-use changes [19,20].

Hydrological models used for peak estimation and hydrographic calculations have evolved in line with the spatial information sources provided by RS and GIS techniques. The Watershed Modeling System (WMS) provides an advanced graphical environment for building a great number of mathematical models used in hydrological and hydraulic calculations, which can be classified into six main models: hydrological (HEC-HMS, HEC-1), hydraulic (HEC-RAS, HY-8), rain drainage networks (EPA-SWMM, XP-SWMM), water quality analysis (EPANET), water quality (HSPE, CE-QUAL-W2), and two-dimensional hydrological models (GSSHA).

The importance of remote sensing is demonstrated by its superior ability to provide abundant Earth information that plays an important role in continuous observations of the Earth and its various resources [21–25]. Satellite images are key documents that help produce maps in both paper and digital spatial distributions. For terrestrial components in a broad framework [26–29], remote-sensing technology and GIS, combined with appropriate models of rainwater flow, provide ideal tools for estimating the volume of direct water flow and peak discharge volume as well as provide a source for water charts [30]. For model input parameters, satellite data can provide us with local information on land use, soil, vegetation, drainage, etc., in conjunction with traditionally measured climate parameters, and also help to study rapidly changing phenomena such as floods. Flood spatial information technologies, particularly geographic information systems and remote sensing (RS) technologies, have proven to be effective tools in monitoring changes in land use [31–33]. In determining drainage patterns and in water resource planning, GIS programs have been widely used in several geomorphological, environmental, and flood management and environmental applications [34–36].

Flood risk mapping and risk analysis of any of the drainage basins involves several factors or criteria [37,38]. The geographic information system (GIS) and remote sensing (RS) applications have contributed significantly to the analysis of natural hazards [39,40]. Over the past few decades, researchers have been involved in developing different methods and models for natural hazard mapping using RS and GIS technologies [41,42], including frequency [43,44], analytical hierarchy [45], fuzzy logic [46], logistic regression [47], artificial neural networks [48–50], evidence weights [51], multi-standard resolution [52,53], and hydraulic modeling, which are essential for flood risk management and mitigation [9,54–59].

Many researchers have addressed the problems of sudden flood risk in different parts of the world in many studies. Khubat and others [60] made a comparative assessment of flood susceptibility

modeling in one of China's most flood-prone areas, the Ningdu Catchment, using multi-criteria decision-making analyses and machine-learning methods. Three multi-criteria decision-making (MCDM) analysis techniques (VIKOR, TOPSIS, and SAW), along with two machine-learning methods (NBT and NB), were tested for their ability to model flood susceptibility. Wang and others [61] investigated the use of a novel hybrid technique by integrating a multi-criteria decision analysis and geographic information system to evaluate flood susceptibility mapping (FSM) in a case study in Shangyou County, China.

Sharma and others [62] used a multi-standard analysis for flood risk assessment of the Kubili River Basin, Assam, India, where a multi-criteria analysis approach (MCA) was introduced to describe the effective use of geospatial techniques for disaster risk reduction at the village level, in order to produce a map of flood-prone areas. Salish and others [63] analyzed the vulnerability of flooding surrounding the Markham River in the Province of Murubi in Papua New Guinea by creating a reasonable sensitivity map of floods. Khabat and others [64] assessed the vulnerability of flooding based on GIS and the establishment of flood vulnerability maps using four models: flood frequency rate (FR), weights (WofE), the analytic hierarchy process (AHP), and a method combining both the frequency rate and analytic hierarchy process methods (FR–AHP). Moreover, they compared the severity of flooding and bivariate statistical models with the use of multi-standard analysis techniques. Getahun and Gebre [65] used GIS techniques and the HEC–RAS hydraulic model to assess the risk of flooding and to map the flooded areas in the Awash River basin in the State of Ethiopia. In this study, the flooded areas along the Awash River were mapped for different return periods based on the highest flows.

Olga and others [66] assessed the risk of flooding in river basin areas in the Murky region in Greece by processing information of seven criteria using multi-criteria analysis in the GIS environment in order to determine flood risk areas within the river basin. Determination of weights for each criterion was carried out using hierarchical analysis (AHP). Clement and Edward [67] used GIS applications, remote sensing, and serial hierarchical analysis of Accra flood modeling through the production of a flood risk map. Martin and others [68] used a flood risk index, based on remote sensing and GIS technology, to describe the risk of flooding in areas where data are scarce, taking into account slope, flow accumulation, drainage network density, distance from drainage channel, geology, land use/cover, rainfall intensity, and the factors causing floods in order to produce a flood risk map. The study of Karim et al. [9] applied a new approach to identify urban areas exposed to the risk of the floods in the city of Tabuk, with the recommendation of utilizing a mechanism for flood prevention and city protection through the integration of hydrological modeling.

Data from [69] indicated that the natural disasters that occurred in Saudi Arabia over the past 15 years (2002–2017) have mostly been floods, and they are expected to recur seven times a year due to rapid urbanization, climate change, and the expansion of cities without clear planning control. Continuous change in the patterns of land uses of Saudi cities at the expense of natural valleys is a serious national problem. What increases the seriousness of this problem in the Saudi Kingdom is that these valleys represent the main places of agricultural, urban services, and economic activities in Saudi cities, thus posing a direct threat to the lives of the population and their economic and service activities. The vast majority of the Kingdom's cities are in valleys or within low areas where valleys end up.

With the urbanization and expansion of land use along the Riyadh–Dammam train path, as a result of the economic boom witnessed by Saudi Arabia in general and the eastern province, this expansion has led to direct and indirect impacts on the nature of the relationship. Between the land use and dry wadies in the region, urbanization has led to an increase in the rates of meandering, explained by the changes in the streams and tributaries of some wadies in more than one place, as a result of this expansion of land use at the expense of these wadies and tributaries.

These unjust encroachments on the wadies and the change of their paths have contributed to an increase, despite the destructive effects, of floods. This has also led to the adoption of urban plans that do not take into account the paths of the wadies and their reefs, including continuous demolition work

by the people and the developers of these schemes, where most of the valleys are exposed. In addition, planning of road networks and railway paths has been carried out without taking into account the trends and inclinations of wadies and tributaries. This is what happened in the study area, which experienced significant changes in land use that led to a change in the direction of the flow of water. The transformation of its run directly to the path of the Riyadh–Dammam train led to the disaster of the drift of the train. Figure 1 shows the derailment of the No. 14 Riyadh–Dammam passenger train on 18 February 2017 as a result of the track's exposure to the torrents of the wadies of the Dil' Al Midra Al Janubi and from the change of land uses in the region. About 18 people were injured, 193 passengers were transported to Dammam city by a reserve train, and the route of the damaged line was closed while the General Railway Corporation began its task to look for the causes of the disaster.

In this study, an innovative approach was used to measure the effective impact of changes in the land use and morphology on the high risk of floods in order to reveal the sustainability of the railway facility. Analyses were conducted with the Riyadh–Dammam train line, Saudi Arabia. Analyses were based on the combination of GIS, remote sensing (RS), and water basin modelling systems (WMS), as well as the hydrological modelling program of the Hydrological Engineers Program (HEC–HMS) and HEC–RAS river analysis system. The proposed planning policies and recommendations will contribute to understanding the nature of floods in these environments that have undergone dynamic changes, which cannot be analyzed using old maps and traditional methods, and alternative preventive measures have been proposed in the study area to help mitigate the effects of sudden floods of the Dil' Al Midra Al Janubi wadi that led to the train disaster.



Figure 1. Cont.



**Figure 1.** The Riyadh–Dammam train derailment. Image (A) shows the Riyadh–Dammam train derailment on 18 February 2017. Image (B) shows overturning of the Riyadh–Dammam train resulting from land drift due to floods.

## 2. Area of Study

The Riyadh–Dammam railway is one of the most important transport axes in the Kingdom of Saudi Arabia. Railways are considered as one of the most important means of transport that countries depend on to achieve their economic, social, and political objectives. With an increase in the economic value of railways, the Saudi Kingdom developed its rail network to connect Saudi cities in different regions. Through the awareness of the Kingdom of Saudi Arabia of the pivotal role of the railway sector and its importance in realizing the vision of the Kingdom of Saudi Arabia 2030, the Saudi Railways Organization (SRO) established the Riyadh–Dammam line to link the Administrative Capital of Riyadh with the Petroleum Capital of the Kingdom in the Eastern Province, Dammam. The Riyadh–Dammam railway, which has a length of approximately 450 km, starts in the city of Riyadh and ends in the city of Dammam in the east of the Kingdom. It is located between latitudes  $24^{\circ}39'4.85''$  and  $26^{\circ}24'26.42''$  N, and longitudes  $46^{\circ}44'41''$  and  $50^{\circ}7'30''$  E, passing through four main stations from west to east: Riyadh, Hafuf, Bqaiq, and Dammam (Figures 2 and 3). The study area chosen along the route of the Riyadh–Dammam railway was exposed to flooding on 18 February 2017, which led to train derailment, overturning, and the loss of lives and property. The area is in the Dhahran western neighborhood, Dammam District, in the Eastern Province of Saudi Arabia. The area exposed to flood risk, where the train derailment accident took place, represents about 3.55 km of the Riyadh–Dammam railway track, and it is an area where significant changes in land use have taken place.

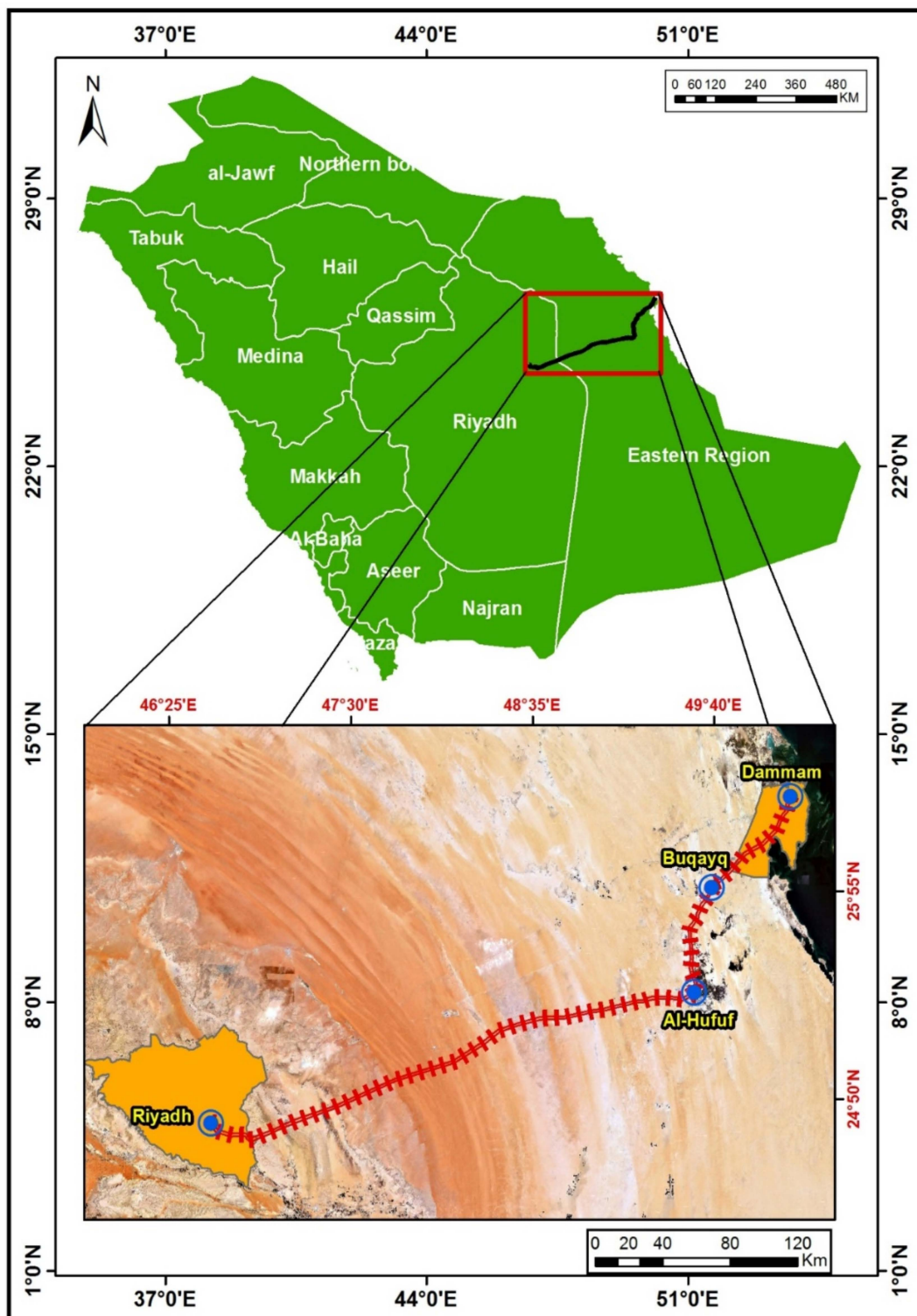


Figure 2. Location of the Riyadh–Dammam train track, Saudi Arabia.

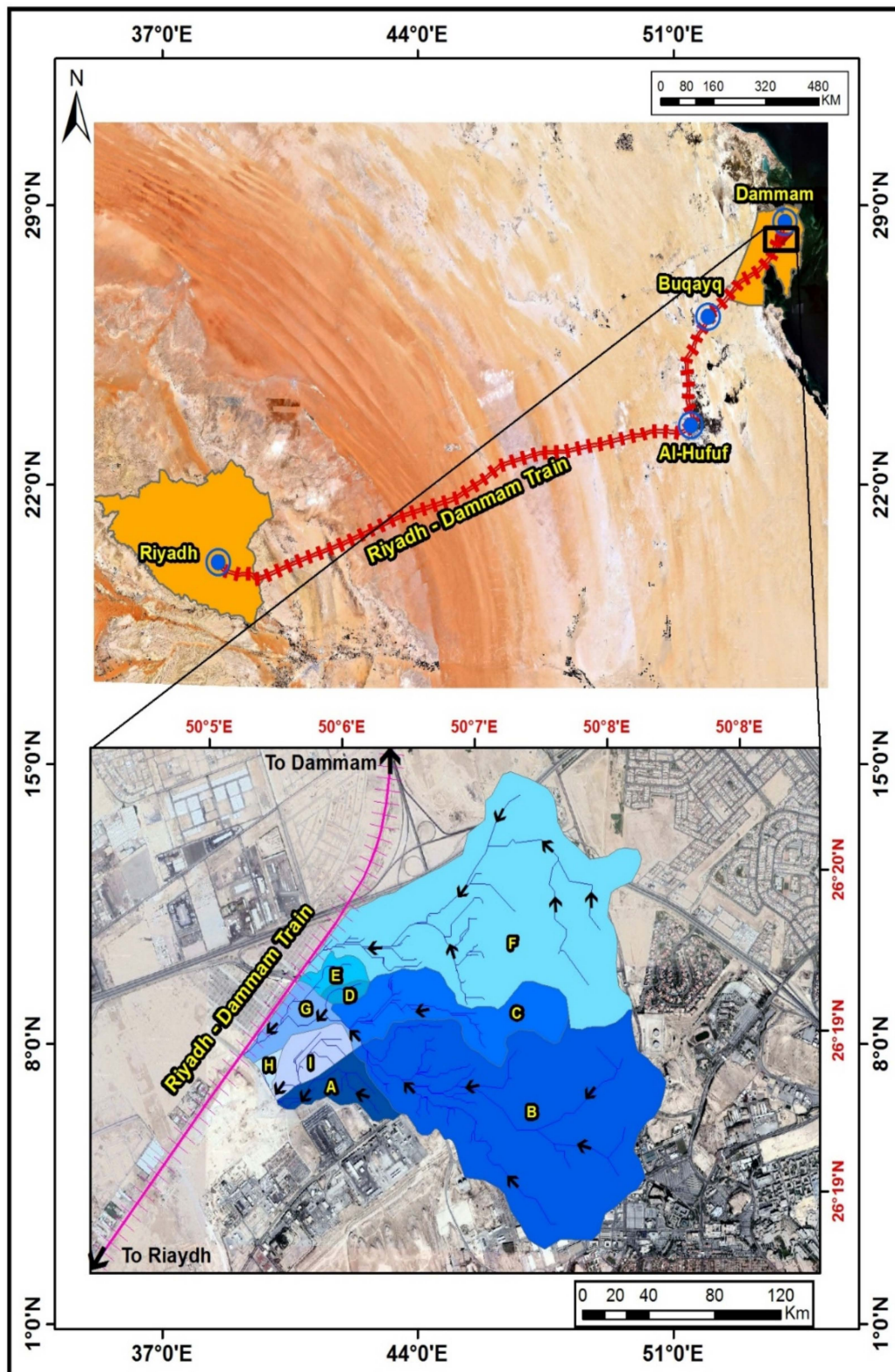


Figure 3. Study area and valleys (A, B, C, D, E, F, G, H, I) affecting the Riyadh–Dammam train track.

### 3. Methodology and Data Processing

#### 3.1. Monitoring the Change in Land Use and the Morphology of the Wadies in the Study Area

##### 3.1.1. Monitoring the Change in Land Services in the Study Area

To determine and monitor the land-use changes in the area where the Riyadh–Dammam train drifted, the program ERDAS IMAGINE 2016 was used, and the process of monitoring changes went through six basic stages. **The first stage** was to download satellite Images (Download Images) through the site of King Abdul Aziz City of science and technology at the Space Research Institute. Images from the satellite ‘Geo-I-1’ were obtained with a resolution of 60 cm for the years 2011 and 2017, periods before and after the train drift accident. This study used multispectral space images. Geo-I-1 spectral images, which include four spectral bands with high spatial resolution, use two types of sensors that provide multispectral images and pan meters with dimensions of 1.65 m × 1.65 m and 0.41 m × 0.41 m, respectively. Type 1 (multispectral) offers a better spectral resolution than that of type II (type II). Panchromatic images, which include four spectral bands (nearby blue, green, red, and infrared), and type II images (panchromatic) offer a better spatial accuracy than the first, with a spatial accuracy of less than 0.5 m. The radiation accuracy of both is 11 bits with a set of brightness values (BVs) from 0 to 2047 (Table 1).

**Table 1.** Features of the SAT “Geo-I-1” satellite images with a resolution of 60 cm for the years 2011 and 2017.

Bands	Spectral Range (μm)	Spatial Resolution (m)	Dynamic Range (bits)
Pan	0.450–0.800	0.5	
Blue	0.450–0.510		
Green	0.510–0.580		11
Red	0.655–0.690	0.2	
NIR	0.780–0.920		

**The second stage**, consisting of the aggregation of spectral bands (Layer Stack) where spectral channels were assembled, was carried out on multiple ranges for each satellite image by the main menu raster, including the spectral icon. Then, the Stack Layer option was dealt with in **the third stage**, and subset image cutting, where the boundaries of the study area were determined, and were cut from the original satellite image for easy handling. **The fourth stage** dealt with spectral enhancement spectroscopy. Spectral enhancement was performed through the raster menu to increase the spectral accuracy and reduce spectral interference, including the spectral icon and principal component option.

**The fifth stage** dealt with supervised classification. The method was directed using maximum likelihood from the raster list, including icon classification and supervised classification. **The sixth stage dealt with** accuracy assessment. During use of the error matrix for the maximum likelihood method and the application of the kappa coefficient, which was also performed by the error matrix, the accuracy was rated using the main menu raster. Classification, including supervised classification, included the accuracy assessment option.

From the edit menu in the accuracy assessment window, random points were added and used to test the accuracy of the classification (number of random sample points = 100 points). Random sample points with a value (zero) that expressed unclassified areas were deleted and unclassified by the order criteria using the equation (Class = 0). Then, choosing select and delete selection, all unclassified samples were deleted, and the sample points were shown on the satellite images by selecting the satellite image window of the view menu and then select viewer. Then, the points were shown on the image by selecting show all from the view list. To calculate the accuracy of the classification after entering the ranks of the report list and the accuracy report, a final report was generated with all the details, which showed the total accuracy of classification and the classification accuracy of each phenomenon (Table 2).

**Table 2.** Classification accuracy of satellite images for 2011 and 2017.

Image Date	Classification			
	Type	Method	Overall	Kappa
2011	Supervised Classification	Maximum Likelihood	93%	0.9
2017	Supervised Classification	Maximum Likelihood	98%	0.97

The total image classification accuracy in 2011 was about 93% of the total samples used in the test, i.e., 7% of the total samples were differently rated when assessing accuracy. The total classification accuracy of the equation is calculated by

$$Overall = \frac{\sum_{i=1}^K xil}{N} \quad (1)$$

where  $N$  is the total number of samples;  $\sum_{i=1}^K xil$  is the total correct samples for all classified phenomena. Kappa coefficient was also about 0.9, and the Kappa coefficient is calculated from the equation:

$$Kappa = \frac{N \sum_{i=1}^K xil - \sum_{i=1}^K (xi + \times x + i)}{N^2 - \sum_{i=1}^K (xi + \times x + i)} \quad (2)$$

where  $N$  is the total number of samples;  $\sum_{i=1}^K xil$  is the total correct samples for all classified phenomena;  $\sum_{i=1}^K (xi + \times x + i)$  is the total product determined by multiplying the total number of samples and the number of correct samples per phenomenon.

For the image rating in 2017, the accuracy of satellite image classification was about 98% of the total samples used in the test, i.e., 2% of the total samples differed when evaluating accuracy, and the kappa coefficient was about 0.97.

### 3.1.2. Monitoring the Change in the Morphology of the Wadies in the Study Area

The digital elevation model was based on a high-resolution digital elevation model through the site of King Abdulaziz City for Science and Technology at the Space Research Institute. Digital elevation models (DEM 1 m for years 2011 and 2017) were obtained for periods before and after the train accident occurred to represent the spatial distribution of heights based on geodetic data, which has proven to be very effective when compared to field and digital height data of stereoscopic images, especially in terms of the processing duration of such data as well as the monitoring of changes. The morphology on the historical geomorphology maps of the study area was on the scale of 50,000:1, provided by the General Authority for Geological Area, where many geomorphological and morphological changes were observed during the period 2011–2017.

### 3.2. Hydrological Modeling

HEC–HMS was applied to calculate hydrograph curves in multiple ways, for both simple and complex drainage basins, by natural or artificial methods. It is one of the programs globally used in the field of hydrology and was developed by the American Army Organization. Using a 24-h storm design, the Soil Conservation Services (SCS) TYPE II distribution was used, and the SCS method was used to calculate the delay and concentration times for different frequency times of 100, 50, 20, and 10 years. The output of the hydrological model used in our study was deduced to infer the hydrograph of the water's drainage basins. It was necessary to use mathematical equations that represented the rain loss or link runoff and total rainfall to calculate the curve number and the greatest drainage ( $m^3/s$ ) (as illustrated in Table 3). The Kirpich equation [70] was used in the calculation of the time of concentration (Equation (1)), which is the time needed for rainwater falling on the surface of the basin to gather, until it reaches the point where the flow is calculated. The delay time was calculated using

the SCS method (Equation (2)), which is the time between the occurrence of a unit of rain and the occurrence of a unit of water runoff. The depth of rain or direct flooding in the basin was calculated to infer the total flooding at the actual rain value (Equations (3)–(5)). The amount of water in the area before the occurrence of a flood, such as the water resulting from infiltration and rainwater found on plants, was also estimated using Equation (4). Equation (2) can be simplified, as illustrated in Equation (5). The maximum soil moisture was calculated using Equation (6), where CN represents the curve number in the Soil Conservation Services (SCS) method. This coefficient depends on land uses and the nature of the soil [71]. The maximum drainage ( $\text{m}^3/\text{s}$ ) of each basin was calculated for different return periods using Equation (7), and greatest drainage time was calculated using Equation (8). All of the aforementioned equations are illustrated in Table 3.

**Table 3.** Equations used in the current study.

Equation	Formula	Description
(1)	$t_c = 0.0195 \left( \frac{L^{0.77}}{S^{0.385}} \right)$	$t_c$ = time of concentration (min); $L$ = maximum flow distance (m); $S$ = maximum flow distance slope (%); $T_{LAG}$ = lag time (hour); $Sr$ = maximum effort of soil moisture (maximum retention), calculated from the curve number (cm); $Y$ = basin slope (%); $P$ = rainfall for different return periods (cm); $Ia$ = amount of water, before the occurrence of a flood, such as filtration and suspended rain on plants; $qp$ = peak discharge ( $\text{m}^3/\text{s}$ ); $A$ = basin area ( $\text{km}^2$ ); $T_p$ = time until the peak (hour); $Q$ = direct runoff (mm); and $\Delta t$ = duration of designed storm water
(2)	$T_{LAG} = \frac{L^{0.8} [Sr+1]^{0.7}}{1900 \sqrt{Y}}$	
(3)	$Q = (P - Ia)2 / (P - Ia + Sr)$	
(4)	$Ia = 0.2Sr$	
(5)	$Q = (P - 0.2Sr)2 / (P + 0.8S)$	
(6)	$Q = (P - 0.2Sr)2 / (P + 0.8S)$	
(7)	$qp = \frac{0.208AQ}{T_p}$	
(8)	$T_p = \Delta t / 2 + T_{LAG}$	

### 3.3. Hydraulic Modeling

Two-dimensional hydraulic modelling was carried out using HEC-RAS, version 5.0.4, of the Center for Hydrological Engineers. The program can calculate the movement of sediments and chemical pollutants in the current, evaluate channels and passes, and assess the distal stalactites. The program is used in mapping the spread of floods and to calculate the risk of floods in threatened places. The applications of the program are used to calculate the rates of degradation and aggradation resulting from the flood water currents. Two-dimensional modeling of the program (HEC-RAS) was employed to calculate the speed, depth, and spread of the Dil' Al Midra Al Janubi wadi flood. Construction of the two-dimensional hydraulic model was achieved using HEC-RAS with four stages: (a) correction or addition of engineering data for transverse sections and hydraulic structures; (b) peak flow data input; (c) general definition of the model plan (engineering data files and flow were set based on the results of previous hydrological modelling and the high 5-m digital height model); and (d) implementation and verification of hydraulic calculations.

The methodology of the study and the data processing shown in Figure 4 can be presented in some detail through six basic steps.

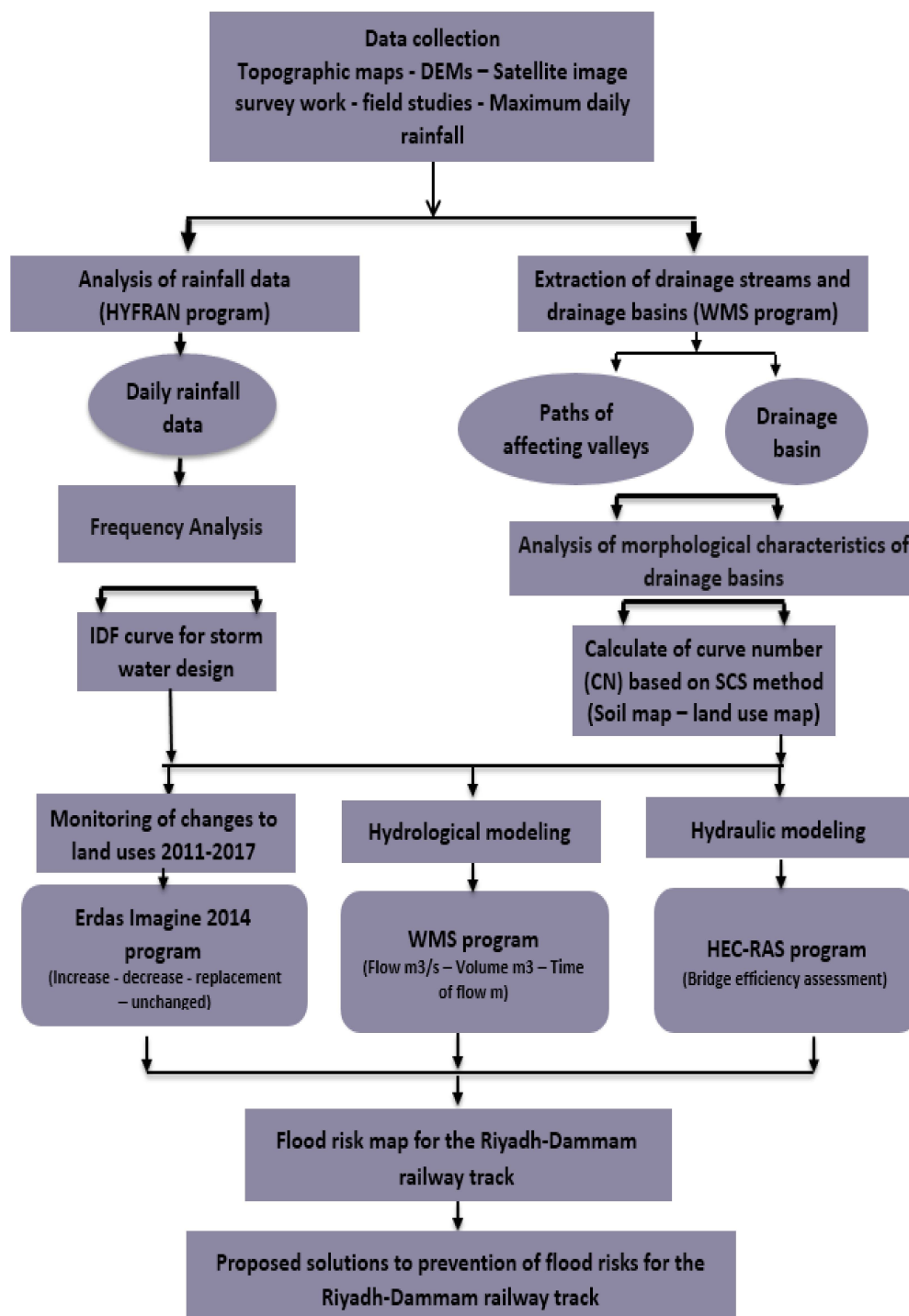


**Figure 4.** Methodology of flood hazard assessment and prevention for the Riyadh–Dammam railway track.

### 3.4. Precipitation Quantity Analysis of the Different Return Periods and Determination of the IDF Curves of Drainage Basins Affecting the Study Area

Precise determination of the amount of rain that has fallen on the water basin is one of the most important factors that helps in the accurate calculation of the floods accumulated from these rains. It is also considered as an accurate basis for water statistic calculations and to calculate the possibility of the recurrence of floods. By reviewing the records of the stations of the Ministry of Water and Electricity

and the General Presidency of Meteorology and Environmental Protection, it was found that the study area is covered by the meteorological station of Dammam (HU001).

The rainfall depth was determined for different return periods (2, 3, 5, 10, 20, 50, and 100 years) using the Hyfran statistical analysis program [72]. Various statistical distributions were applied (e.g., Normal, Log-Normal, Log-Pearson Type III, Pearson Type III, Gumbel, and Exponential). It was concluded that the Gumbel method was the optimal method for the Dammam Meteorological Station (HU001) (Figures 5–7 and Tables 4 and 5).

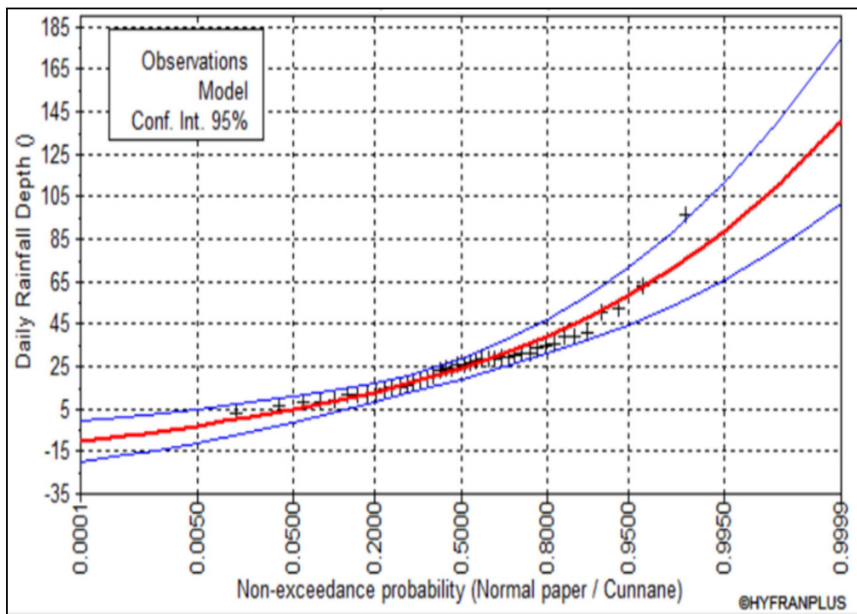


Figure 5. Probability distribution curves at Dammam Station (HU001) of the maximum daily data using the Gumbel method.

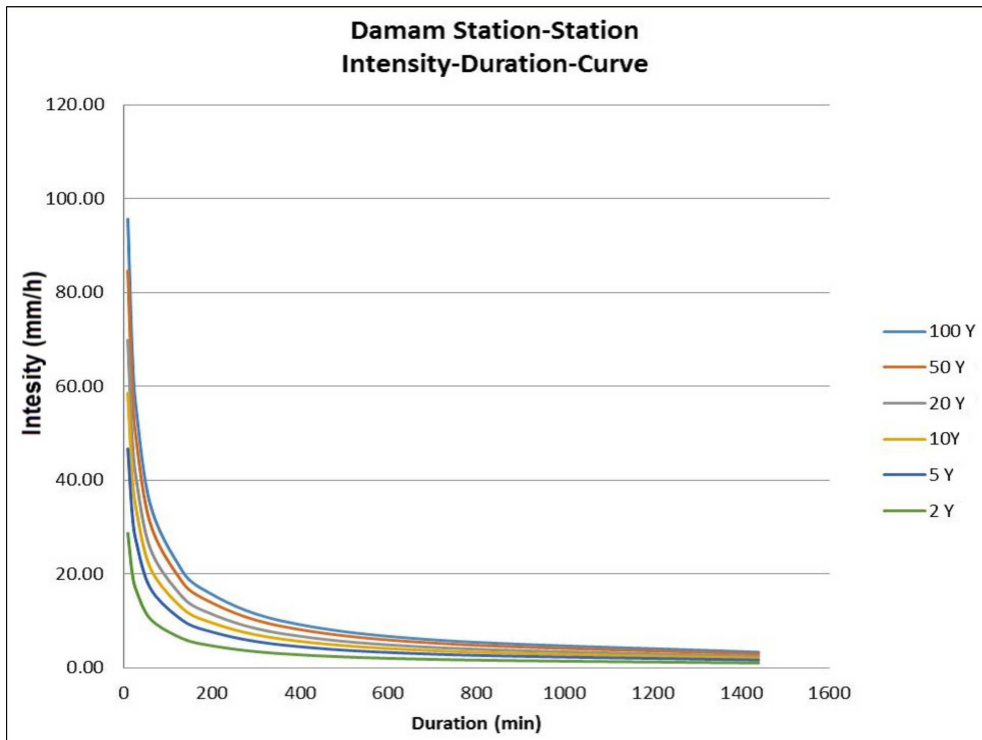


Figure 6. Intensity–duration–frequency (IDF) curves of Dammam Meteorological Station (HU001).

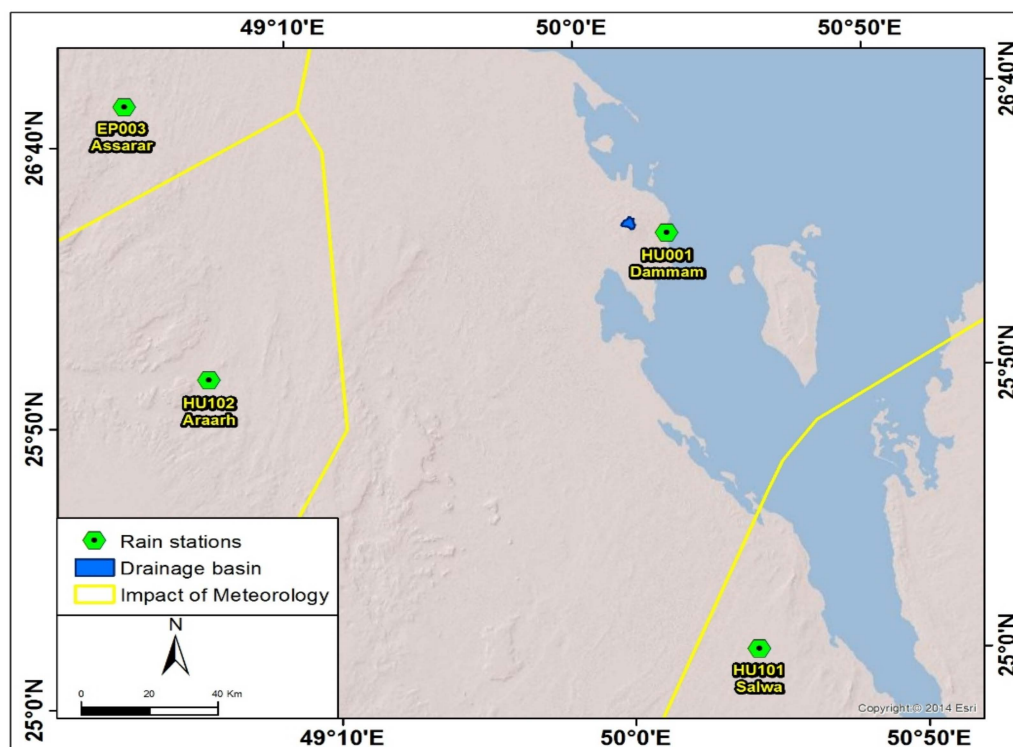


Figure 7. Sites of the surrounding meteorological stations representing the study area.

Table 4. Statistical distribution of rainfall of the Dammam Metrological Station (HU001) at different return periods.

Statistical Distribution	Rain Depths at Different Times						
	2	3	5	10	20	50	100
Log-Normal	22.2	29.4	38.5	51.3	65.1	85.2	102
Log-Person Type III	23.7	30.9	38.8	48.3	56.9	67.1	74.0
Person Type III	23.6	30.8	38.4	48.0	57.1	68.4	76.7
Gumbel	23.9	31.0	38.9	48.8	58.2	70.5	79.7

Table 5. Rainfall depths of different return periods at Dammam Station (HU001).

Return Period (Year)	2	3	5	10	20	50	100
Rainfall within 24 h (mm)	23.9	31.0	38.9	48.8	58.2	70.5	79.7

### 3.5. Morphological Characteristics of Drainage Basins Affecting the Study Area

The morphology of the drainage basin was analyzed using the Watershed Modeling System (WMS) through the Drainage Module (computes basins data). The morphological characteristics of the basins were calculated automatically. These characteristics can be found through the “display option”. Nine basins belonging to the main valley of Dil’ Al Midra Al Janubi affected the study area, which included A, B, C, D, E, F, G, H, and I. These basin areas ranged from 3.164 km<sup>2</sup> (basin (F)) to 0.041 km<sup>2</sup> (basin (H)). Basin (F) was the longest (5.1 km), while basin (H) was the shortest (393 m). The slopes of basins ranged from 0.030 m/m (basin (C)) to 0.006 m/m (basin (G)) (Table 6 and Figure 8).

### 3.6. Hydraulic Groups of Soil and Land Uses for the Drainage Basins Affecting the Study Area

One of the main coefficients to calculate the curve number (CN) is the definition of the hydrologic group of the soil and land uses, as the value of the curve number depends mainly on these two variables. The SCS method has identified four hydrological groups of soil [71] according to the rate at

which water is transferred through it. These groups are A, B, C, and D, and each group has its own characteristics regarding the surface runoff. The area of the present study was within the geology of the West Arabian Gulf square (LE-208).

**Table 6.** Morphometric characteristics of drainage basins in the study area affecting the Riyadh–Dammam train track.

Basin Name	Basin Area (km <sup>2</sup> )	Length (m)	Basin Slope (m/m)	Average Level (m)	Lag Time (min)	Concentration Time (min)
A	0.287	1430	0.013	47.50	16.4	27.3
B	3.441	3328	0.018	79.00	27.9	46.4
C	0.857	2161	0.030	79.50	16.4	27.3
D	0.061	459	0.024	51.50	5.4	9.1
E	0.120	652	0.017	51.50	8.1	13.6
F	3.614	5085	0.014	74.50	42.6	71.0
G	0.296	1410	0.006	44.00	22.4	37.4
H	0.041	393	0.015	42.00	5.7	9.6
I	0.269	1055	0.009	43.00	14.7	24.6

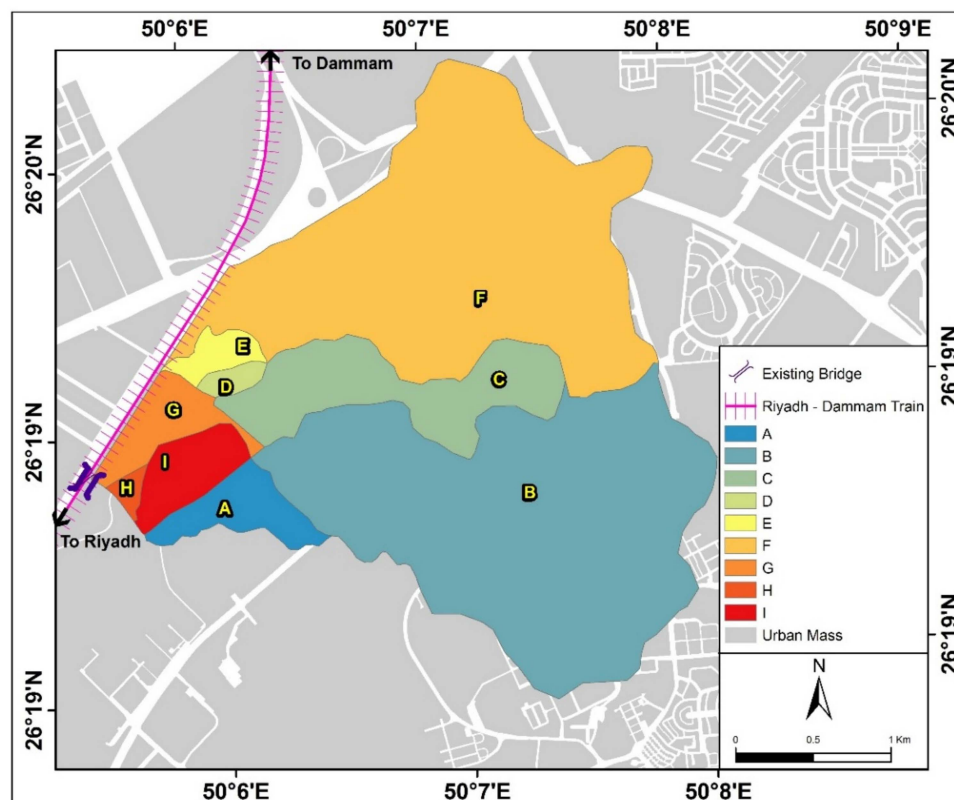


**Figure 8.** Drainage basins in the study area affecting the Riyadh–Dammam train track.

Through the analysis of geological maps and satellite images, it was observed that the geology of the study area was characterized by the geological features that are shown in Figure 9. The geological units in the study area can be described in detail as follows: sandy areas with an area of about 0.085 km<sup>2</sup>, rocky ridges with an area of about 0.65 km<sup>2</sup>, gravel with an area of about 7.4305 km<sup>2</sup>, and wind-formed soil with an area of 0.8145 km<sup>2</sup>. The sub-drainage basins were represented in the hydrological group of soil (A), which is a disintegrated, highly permeable soil (Figure 10).

Land uses were acquired by the classification of satellite Geo-I-1 images using ERDAS IMAGINE software. Land-use layers were defined by the WMS program by introducing the land-use layer after

its definition by selecting new coverage in GIS data and then selecting add shape file data. There was one category of land use for sub-drainage basins, which was urban development lands.

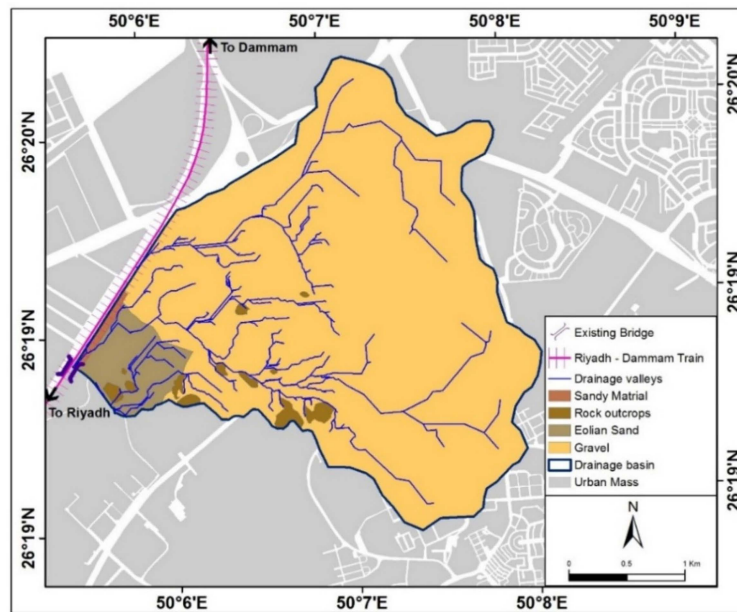


**Figure 9.** Geological map of drainage basins in the study area affecting the Riyadh–Dammam train track.

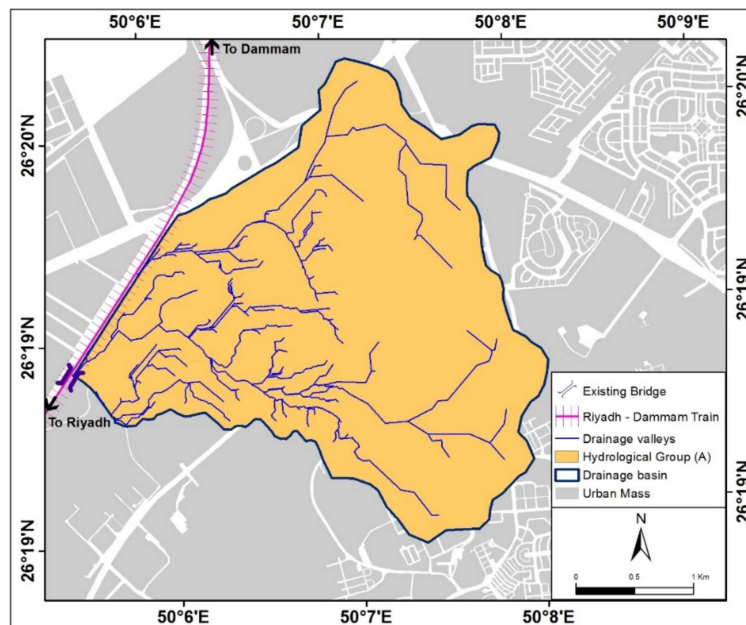


**Figure 10.** Hydrological soil group of drainage basins in the study area affecting the Riyadh–Dammam train track.

### 3.7. Curve Numbers of the Drainage Basins Affecting the Study Area

The WMS model provides several hydrological models, the most important of which are HEC-1 and HEC-HMS. Each of these models provides equations for calculating losses and infiltration, the most important of which are the uniform loss method (LU); exponential loss (LE) Method; Green and Ampt (LG) method, which is used to calculate the losses (particularly soil infiltration); the Holtan (LH) method; and the method of managing soil maintenance services for loss calculation (SCS loss method (LS)). One of the most widely used methods in estimating the quantities of water lost by infiltration of the subsoil was used. This method is called curve number (CN) and is based on three elements: the

precondition of soil moisture, soil coverings, and the hydrological groups of soil. The value of CN ranges from zero to 100, which reflects the response of water to the components of the land cover types in the drainage basins, thus expressing the degree of soil solidness. The higher the CN the lower the permeability is [73–77] (Table 7).

**Table 7.** Curve numbers of drainage basins of the study area by soil distribution and land use.

Basin Name	Basin Area (km <sup>2</sup> )	Area of Urbanized Land (km <sup>2</sup> )	Curve Number
A	0.287	0.287	88
B	3.441	3.441	88
C	0.857	0.857	88
D	0.061	0.061	88
E	0.120	0.120	88
F	3.614	3.614	88
G	0.296	0.296	88
H	0.041	0.041	88
I	0.269	0.269	88

### 3.8. Flood Volume Estimation

The HEC–HMS model was applied using a 24-h design and SCS TYPE II. The SCS method was used to calculate the delay and concentration time for different return periods of 10, 20, 50, and 100 years. The results of the hydrological model used in the study were used to identify the hydrograph of the flood waters of the different drainage basins. Hydrograph analysis of the different drainage basins showed that the volume of the floods ranged between 2100 and 185,400 m<sup>3</sup>. Drainage basin (F) was the largest basin regarding flood volume, which reached 185,400 m<sup>3</sup>; basin (H), on the other hand, had the smallest flood volume, which reached about 2100 m<sup>3</sup> (Table 8).

**Table 8.** Flood characteristics of the drainage basins in the study area affecting the Riyadh–Dammam train track for different return periods.

Basin Name	Description	Return Periods (Years)			
		10	20	50	100
A	Peak discharge (m <sup>3</sup> /s)	1.86	2.47	3.29	3.92
	Flood volume (m <sup>3</sup> )	7000	9300	12,400	14,800
B	Peak discharge (m <sup>3</sup> /s)	15.76	21.06	28.08	33.47
	Flood volume (m <sup>3</sup> )	84,100	111,300	14,800	176,900
C	Peak discharge (m <sup>3</sup> /s)	5.55	7.38	9.84	11.70
	Flood volume (m <sup>3</sup> )	21,000	27,700	37,000	44,100
D	Peak discharge (m <sup>3</sup> /s)	0.62	0.82	1.08	1.28
	Flood volume (m <sup>3</sup> )	1500	2000	2600	3100
E	Peak discharge (m <sup>3</sup> /s)	1.09	1.43	1.70	2.26
	Flood volume (m <sup>3</sup> )	2900	3900	5200	6200
F	Peak discharge (m <sup>3</sup> /s)	12.22	16.30	21.82	26.02
	Flood volume (m <sup>3</sup> )	88,200	116,500	155,500	185,400
G	Peak discharge (m <sup>3</sup> /s)	1.57	2.09	2.80	3.33
	Flood volume (m <sup>3</sup> )	7200	9600	12,800	15,200
H	Peak discharge (m <sup>3</sup> /s)	0.41	0.54	0.72	0.85
	Flood volume (m <sup>3</sup> )	1000	1300	1800	2100
I	Peak discharge (m <sup>3</sup> /s)	1.86	2.46	3.28	3.90
	Flood volume (m <sup>3</sup> )	6600	8700	11,600	13,800

### 3.9. Estimation of the Maximum Flood Inflow

The maximum flow rate of the valley basin in the study area varied because of the differences in the amount of rainfall in the drainage area of each basin. Therefore, the maximum flow rates of the project site ranged between 0.85 and 33.47 m<sup>3</sup>/s. Drainage basin (B) occupied the first place in terms of maximum flow rate, which reached about 33.47 m<sup>3</sup>/s (Table 8).

## 4. Results and Discussion

### 4.1. Monitoring Land Use Changes of the Study Area During the Period 2011–2017

In the present study, Geo-I-1 satellite images of the years 2011 and 2017 were used to monitor land-use change. These satellite images were acquired from the King Abdulaziz City of Science and Technology, Space Research Institute. The classification process was conducted using the maximum likelihood method. Classification accuracy of the satellite images was carried out. Moreover, time change detection of each phenomenon classified according to different calculations and quantitative indicators was done. Table 9 and Figure 11 illustrate the most important features of land-use changes in the area where the Dammam train derailment took place.

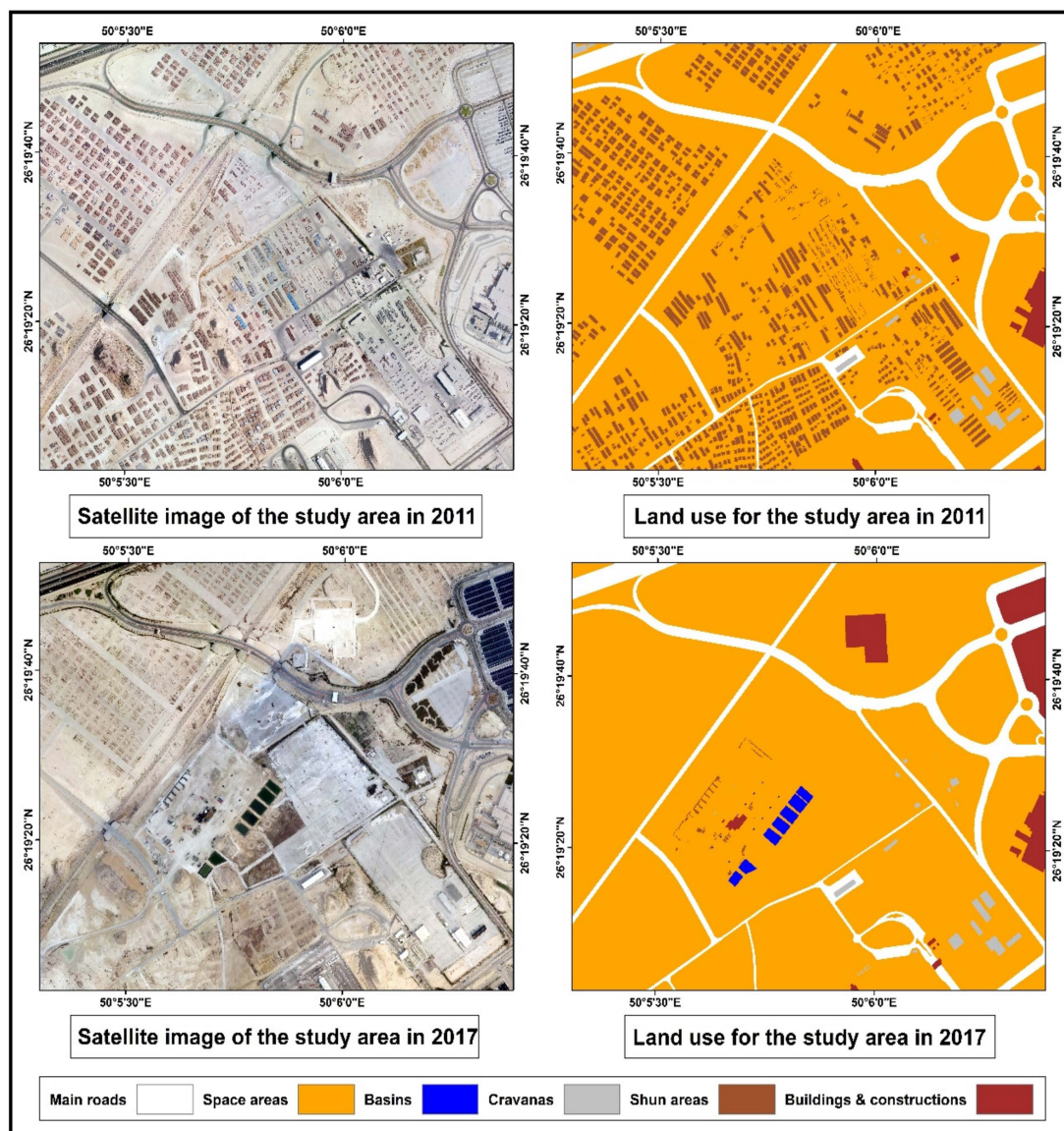


Figure 11. Land use changes in the Dammam train derailment area during the period 2011–2017.

**Table 9.** Features of land use changes in the Dammam train derailment area during the period 2011–2017.

Phenomenon	2011 (Hectares)	2017 (Hectares)	Changes During 2011–2017 (Hectares)	
			2011	2017
Buildings and constructions	2.5	9.8	2.5	9.8
Storage basins	0	1.5	0	1.5
Water store areas	98.2	0	98.2	0
Caravans	18.1	15.1	18.1	15.1
Vacant areas	163.1	255.5	163.1	255.5
Main roads	28.6	28.6	0	0
Total	310.5	310.5	0	0

#### 4.1.1. Monitoring Changes in the Area of Buildings and Facilities

The area of buildings and facilities in 2011 reached about 2.5 hectares, most of which were administrative buildings concentrated in the eastern region of the study area. This area increased during the period from 2011 to 2017, reaching 9.8 hectares, an increase of 292% compared to 2011. This significant increase occurred in some facilities established in the Eastern Province as parking spots. There is no doubt that this significant increase played a crucial role in the morphologist change of land use and was a clear point of objection in the way of wadies.

#### 4.1.2. Monitoring Changes in Store Areas

Store areas occupied about 98.2 hectares in 2011 and were concentrated in most of the study area, especially in the western and southern regions. This area disappeared during the period from 2011 to 2017 and became a vacant area in 2017.

#### 4.1.3. Monitoring Changes in the Vacant Area

Vacant areas occupied about 163.1 hectares in 2011. This area increased during the period from 2011 to 2017, reaching 255.5 hectares, an increase of 56.65% compared to 2011.

#### 4.1.4. Monitoring Changes in the Area of Caravans

The area of mobile caravans was about 18.1 hectares in 2011 and was spread throughout the study area, especially in the southeast. This area decreased during the period from 2011 to 2017, reaching 15.1 hectares, a decrease of 16.57% compared to 2011.

#### 4.1.5. Monitoring Changes in the Area of Water Storage Basins

The area of water storage basins in 2011 occupied about 0 hectares and largely did not exist in the study area. Water storage basins appeared in 2017, where they reached 1.5 hectares, and these modern facilities, which changed the morphology of the wadies in the study area, are one of the most important reasons for the occurrence of train derailment.

Figure 11 shows land uses in the study area between 2011 and 2017. The total area of the common region between the two images was 4.7 km<sup>2</sup>. The area of unchanged land use was 2.7 km<sup>2</sup>, occupying 57.446% of the total area in the region. The decrease in land use was 0.93 km<sup>2</sup>, representing 19.79% of the total area of the region. The increase in land use represented 0.489 km<sup>2</sup>, about 10.404% of the total area. Replaced land use was about 0.128 km<sup>2</sup>, representing 2.723% of the total area of the region. The construction of seven water storage basins, totaling 1.5 hectares, and the increase in the area of construction buildings by about 292%, from 2.5 hectares in 2011 to 9.8 hectares in 2017, are the most important features of the land-use changes during the period 2011–2017 and are the main reasons for the change in the paths of land use during 2011–2017. The run-off of the Wadi Dil' Al Midra Al Janubi caused the Riyadh–Dammam train to drift on 18 February 2017 at the 10 km mark in the west of the Dhahran neighborhood.

#### 4.2. Morphological and Topographic Characteristics of the Valleys Affecting the Study Area that Changed During the Period 2011–2017

Many field studies have been carried out in the study area and its environs by identifying the area's relationship with the surrounding drainage streams, inspecting ferries and bridges on the surrounding roads when conducting detailed studies, and identifying the paths and effects of the valleys passing through the study area. At present, it has been shown through field study and analysis of high-resolution satellite images (Figure 12) that the current study site had some sinkholes, which may capture surface drainage from running or standing water but may also form in high and dry places in a certain location. The mechanisms of sinkhole formation involve natural processes of erosion, gradual removal of slightly soluble bedrock (such as limestone) by percolating water, the collapse of a cave roof, or a lowering of the water table. Sinkholes often form through the process of suffusion. Thus, for example, groundwater may dissolve the carbonate cement that holds sandstone particles together and then carry away the lax particles, gradually forming a void. Occasionally a sinkhole may exhibit a visible opening into a cave below. Water erosion was also observed, which occurs as a result of rainfall on naked soil without the presence of any plants to hold the soil granules or the remains of plants that protect the soil from the impact of rainfall. This type of drift especially occurred in steep areas.



**Figure 12.** Aspects of the field study: geomorphological changes and hydraulic installations in the study area.

As noted from field studies, there are some valleys that pass through the project area, which includes the Dil' Al Midra Al Janubi wadi coming from the east, north, and southeast of the site. In the project area, traces of water and flow tend to appear in some aspect, especially the effects of erosion in the northwest and southwest, as many geomorphological features as well as hydraulic projects such as ferries and bridges exist to the east and north of the project site. The site is monitored by 10 ferries distributed to the east, southeast, and northeast of the project site, including ferries directly at the study location. One bridge is located to the east of the railway line, and another is located west of it, which is very dangerous in terms of facing the site and crossing large amounts of water directly. Two channels were monitored that were located southeast of the project site, including a channel directed towards the study site. Figure 13 illustrates part of the repairing process for the Dammam–Riyadh train track in the study area, while the General Railway Corporation began its work in rehabilitating the track after the crash.



**Figure 13.** Images (A-D): Aspects of the repairing process for the Dammam–Riyadh train track in the study area.

#### 4.2.1. Topographic and Morphological Characteristics of the Wadies in 2011

From a topographical point of view, the physical land levels of the study area ranged from an average of 39 to 53 m, where the eastern part was characterized by a higher altitude ranging from 50 to 53 m. The land sloped generally from east and north to south, where the levels in the south ranged from 39 to 41 m and were considered the lowest areas in the study region (Figure 14). It has been shown that the study area was affected by the passage of the Dil' Al Midra Al Janubi wadi coming from the east and northeast towards the south of the study area, which it intersected. The important thing here is that the wadi in 2011 did not intersect the Dammam–Riyadh train track, and the morphology was not affected by changes in the land use.

#### 4.2.2. Topographic and Morphological Characteristics of the Wadies in 2017

The topography of the study area ranged from an average of 38 to 63 m (Figure 14), which indicated an increase in the height of the physical land levels in the center of the area almost as a result of the aggradation processes and the construction of a concrete layer in preparation for the construction of water storage basins.

There were some small elevations located to the south of the site, which ranged in height from 60 to 63 m. Elevations in the eastern part of the site ranged from 46 to 48 m. Levels of the southern part in the study area ranged between 38 and 40 m and this part was considered the lowest area of study. It is noted here that there was a change in the morphology of the wadis, resulting from the change in the levels of the physical characteristics of the earth where the flow of water to the north was redirected towards the train.

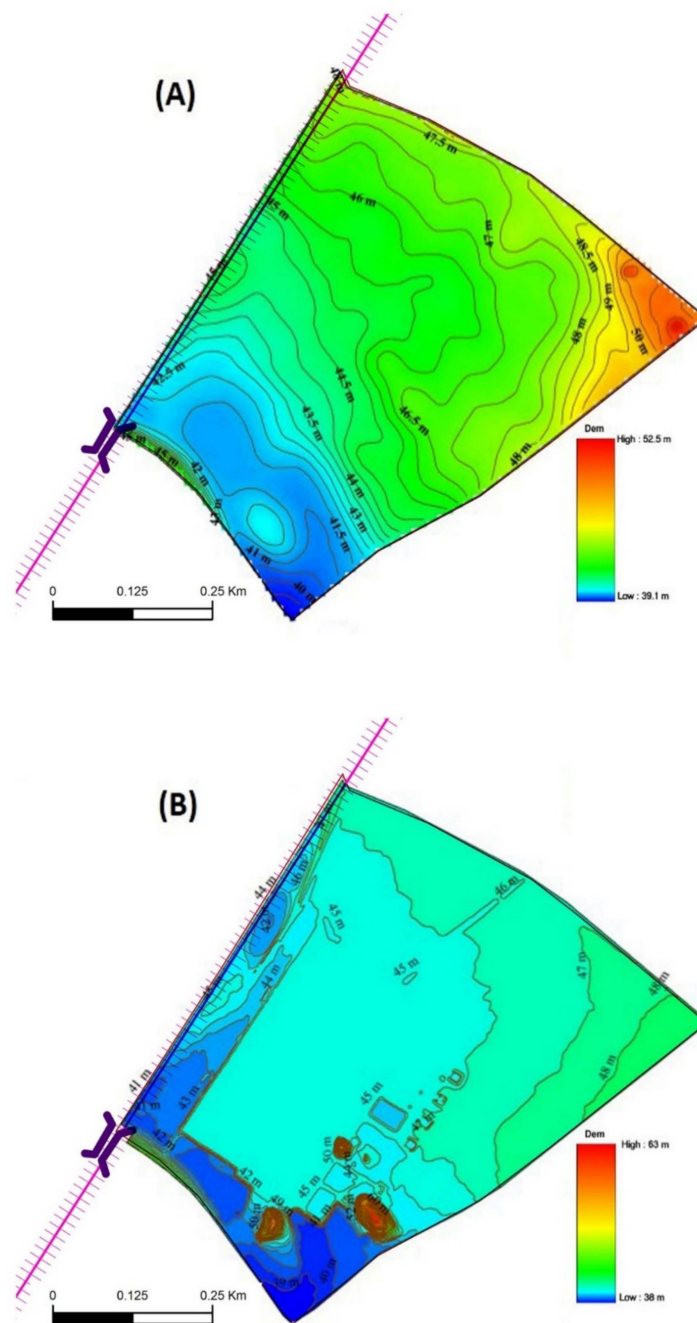


**Figure 14.** Topographic changes in the study area: (A) topographic area in 2011 and (B) topographic area in 2017.

Figures 15 and 16 show the changes in the topography of the study area and the morphology of the network of the main wadies between 2011 and 2017 through digital elevation models. The most notable feature was the change in the elevation of land, both rising and falling, as a result of the urban structures implemented in the study area. This had a significant impact on the change in the direction of the water flow, especially in the change in the direction of the main flow of the wadies from east to southwest, i.e., the orientation of water before development was southwest at a level of 39 m, but urban development and changes in the levels of the earth led to a trend where flow was redirected to the main wadies and became a large part of the direction of flow. This also impacted development in the northwest, i.e., towards the train track, which was dangerous, especially since the urban structures that were developed raised the levels of land in the middle part at least 1 to 2 m.

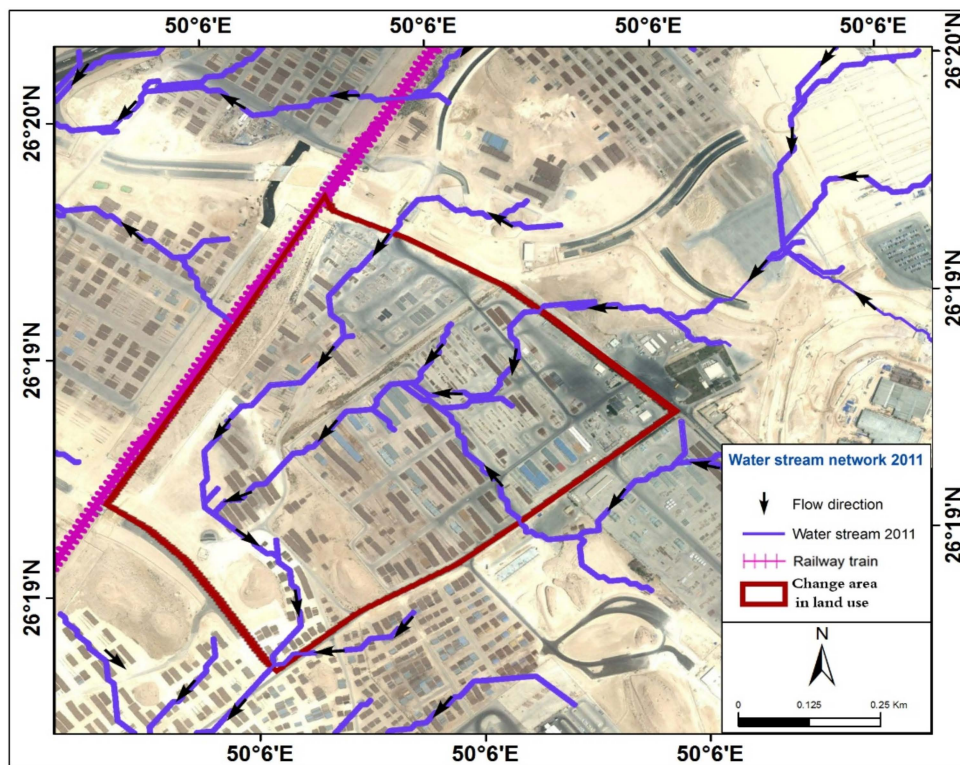


Figure 15. Morphological changes of the wadies network in 2011.

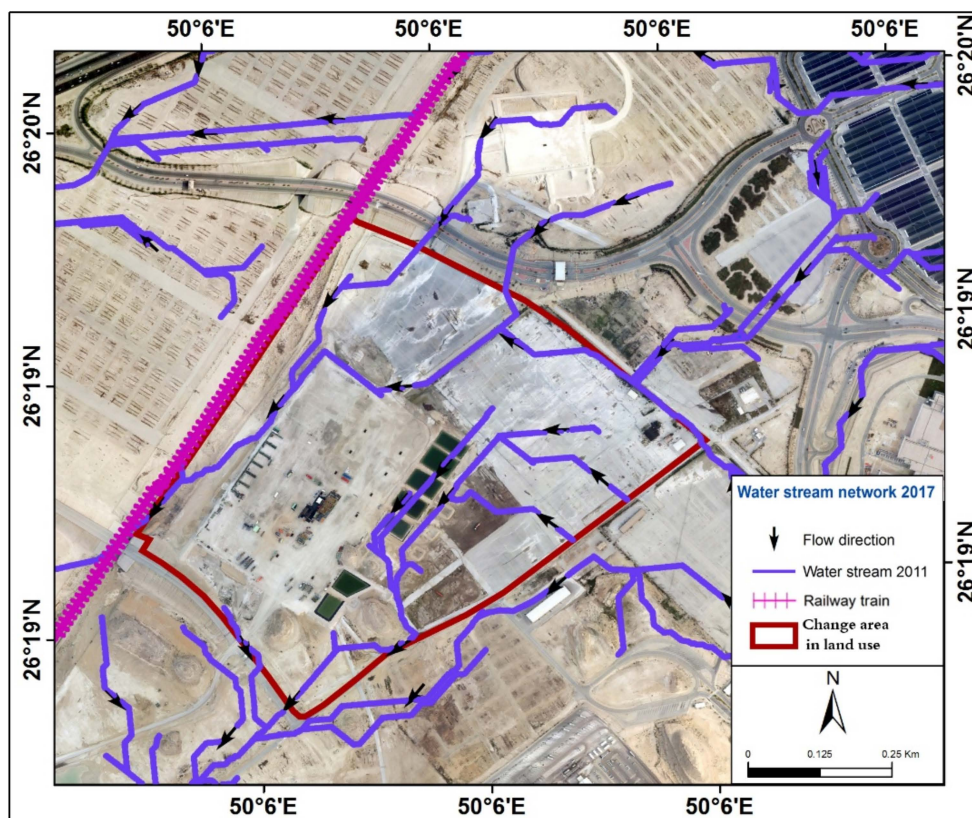


Figure 16. Morphological changes of the wadies network 2017.

#### 4.3. Changes to the Characteristics of Flood Wadies Affecting the Study Area During the Period 2011–2017

The results of the hydrological analysis showed that the study area was surrounded by nine collection basins of different sizes and morphological characteristics, coming from the east, northeast, and southeast with flows ranging from 8.5 to 33.47 m<sup>3</sup>/s, lengths ranging from 393 to 5085 m, and depths ranging from 393 to 5085 m. The site was between 0.10 and 1.41 m, and the water speed was between 0.25 and 3.97 m/s, where the valleys and waterways resulting from these basins intersected with the Riyadh–Dammam train track directly due to the changes in land use. A second-dimensional model was built using the HEC–RAS hydraulic program based on the high-resolution digital elevation model, and the flow results approved for hydraulic modelling can explain the most important characteristics of wadi flooding before the drift accident in 2011 and after the drift accident in 2017.

##### 4.3.1. Hydraulic Analysis of Flooding in 2011

The results proved that the flood caused by wadies and waterways entered the study area from the northeast and southeast borders and exited through one exit in the southwest away from the Riyadh–Dammam train track. The existing hydraulic installations directed the flood water internally. The analysis showed that the flood plain in the internal part of the site had a depth of 0.21 m to 1.41 m, with a speed of 0.32 m/s and 3.99 m/s. This location was also affected at the southwest side of the study area by a local assembly basin, resulting in a flood of depth ranging from 0.10 m to 0.94 m and speed ranging from 0.25 m/s to 3.97 m/s (Figure 17).

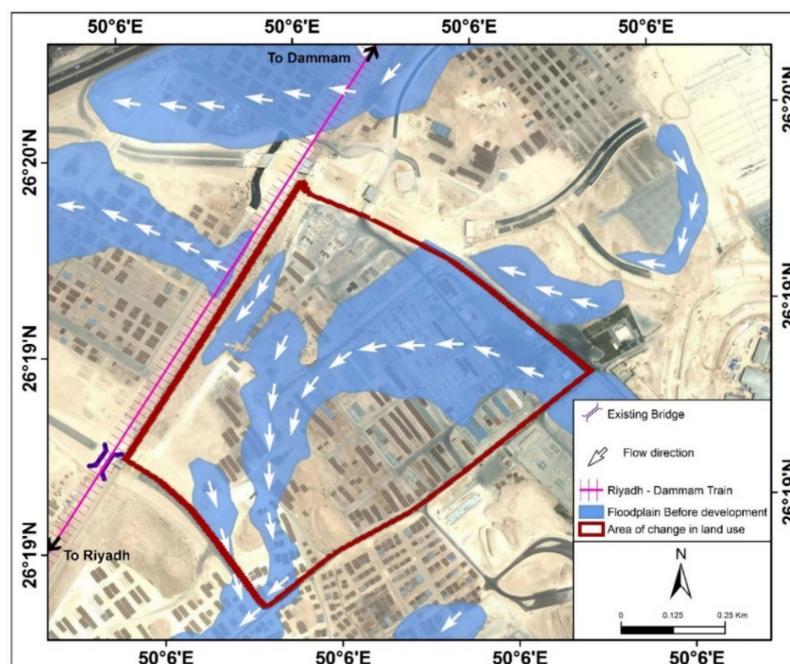


Figure 17. Flooding characteristics of wadies prior to land-use changes in the study area in 2011.

##### 4.3.2. Hydraulic Analysis of Flooding in 2017

Hydraulic analysis in 2017 (Figure 18) revealed a clear change in flood morphology, especially with regard to the form and direction of the flow, as the floodwaters intersected with the Riyadh–Dammam train track at two locations. The first site was at the corner of the study area in the northwest where the water intersected with the railway. The flood water at that point was 1.86 m deep and had a speed of 0.43 m/s.



**Figure 18.** Flooding characteristics of wadies after land-use changes in the study area in 2017.

The second location was at the corner of the study area on the southwest side where the water intersected with a standing road. The flood waters at that point had a depth of 0.57 m and a speed of 4.91 m/s, which confirmed the results of the analysis to calibrate the hydraulic model developed for the flood of the Dil' Al Midra Al Janubi wadi.

Thus, the results of the hydraulic modelling of HEC–RAS confirmed that the flood caused by wadies and waterways attacked the train path at the 10 km mark from the northeast and southeast, and existing hydraulic installations led the flood water to attack this path. Results of the hydraulic analysis of the two previous figures (Figures 17 and 18) indicated that two things helped to increase the risk of floods. The first is the change of the paths of the wadies affecting the study area, where the change intended here is a spatial change and not quantitative. The second is the existence of many hydraulic installations (ferries, bridges, and canals) that run directly into the train track. The site then became a collection point for water coming from the southeast and northeast, which is extremely dangerous.

## 5. Recommendations

- Managing the flood risks of the Riyadh–Dammam railway tracks requires integrated expertise and techniques capable of identifying and analyzing the rapid variables affecting urban growth and land-use change. This contributes to the understanding of the nature of floods in these environments that have undergone dynamic changes, in which old maps and traditional methods are inappropriate to use in conducting applied studies that can effectively cope with the dynamics of floods and urban growth. Hence, the significance of this study lies in its application of a new approach that links the monitoring of changes in the land-use map by remote sensing techniques to the two-dimensional model of the depth, velocity, and spread of floods based on HEC–RAS hydraulic modeling. The study also provides a two-dimensional model for the flow, depth, and velocity of floods; these characteristics are not available in the one-dimensional model of flood runoff.
- The recommendations of the study give priority to implementing protection plans against flood risks and the protection of infrastructure by the frequent maintenance of existing water drainage facilities represented by the bridges. The study also recommends an engineering intervention.

- The proposed alternatives all depend on the concept of adopting concrete channels to guide the intercepted flow to a proposed culvert at the southwest corner of the study area. Channels are considered as the most practical flood mitigation method in urbanized areas since they contain and control the spread of water. The use of dikes, walls, and raising the study area would most probably protect the study area; however, these have several negative aspects in areas such as this. The use of walls and dikes would not completely protect the study area since gaps must remain so that access to the study area is possible, and flood water would enter the study area at these locations. Raising the study area would solve the access problem; however, it would allow the flood water to collect and spread in the surrounding study area, thus causing damage to the surrounding areas. Other possible solutions include the use of detention tanks or detention ponds; however, these hydraulic structures would have to be extremely large in size to contain the flood water generated by the 100 year design storm, which totals 276,200 m<sup>3</sup>. These structures would also require a discharge point to allow for any excess flow; thus, channels and outlet points are needed as well. Based on the above, proposing a series of channels and a culvert that discharges to a natural stream is the most practical solution for this study area and its conditions.
- The study also recommends an engineering intervention through the implementation of two scenarios to manage the flood risks of the Riyadh–Dammam railway. **The first scenario** suggest two concrete, trapezoidal channels. These channels receive the floodwater of the affected catchment basins and lead it to a proposed culvert drainpipe in the southeast of the study area. The proposed channel no. 1 receives flow from the WA, WB, WC, and WI catchment basins and leads them to the proposed culvert drainpipe. The proposed channel no. 2 receives flow from the WD, WE, WH, and WG catchment basins and leads them to the proposed culvert drain pipe. Figure 19 shows the proposed protection plan of the first scenario. **The second scenario** suggests four concrete, trapezoidal channels, which receive the floodwater of the affected catchment basins and lead it to a proposed culvert drainpipe in the southeast of the study area. The proposed channel no.1 receives flow from the WB and WC catchment basins and leads it to the proposed channel no. 3. The proposed channel no. 2 receives flow from the WD and WE catchment basins and leads it to the proposed channel no. 3. The proposed channel no. 3 receives the flow quantities from the WA, WH, and WI catchment basins, as well as the flow from channels no. 1 and no. 2, and leads them to the proposed culvert drainpipe. Channel no. 4 receives the flow resulting from the WG catchment basin and leads it to the proposed culvert drainpipe. As shown in Figure 20, in economic, environmental, and urban aspects according to the models of evaluating alternatives, script no. 1 is the closest to implement in the nature of the region, so the study recommends the implementation of script no. 1 to combat the flood risk in the south Dil' Al Midra Al Janubi wadi valley while preserving the rest of the physical valleys, as they do not interfere with the stream paths.
- The study recommends the necessity of executing the decree issued by the Council of Ministers on 21 May 2007, which specified the controls and procedures to be taken to address flood damage. The decree also outlined the adoption of hydrological studies, not to grant permits to work in the valleys except in coordination with the relevant authorities, and to obligate the permit holders to repair any damage caused as a result of their work, where they should not exceed the limits of the permit given to them, taking into account the total flooding and its paths. Maintenance of drainage networks in tunnels and neighborhoods, and maintenance of culvert drain pipes and bridges before and during rainy seasons, should take into account the quantities and routes of floods when developing roads, bridges, and water tunnel projects inside and outside cities, maintaining flood drainage systems in tunnels and neighborhoods, and maintaining water tunnels and bridges before and during the rainy season.
- Hydrological and hydraulic models used to take into account the dynamics of land cover and land use, especially the urban growth of cities in the plains and valleys where run-off coefficients of urban areas may be doubled from other ground units. This accelerates the need for pre-planning

of cities that grow at the expense of plains and valleys in dry areas, and it is necessary to identify routes for active channels of the floods and prevent encroachments on them, bearing in mind that their dimensions are sufficient to drain the high-frequency torrential water.

- The process of changing the paths of the valleys in designing studies and calculating the amount of runoff of the valleys subject to course changes should be linked to the directions of the current and future land-use schemes, so that urban development can be directed away from the risks of floods.
- It is necessary to conduct an integrated hydrological study of the whole length of the Riyadh–Dammam railway, which is 450 km long, to identify the roads and bridges and culvert drain pipes inside and outside the cities. With the potential risk of floods due to continuous land use changes around the train track, the study also recommends that the results be presented to decision-makers to prevent the problem of train derailment.

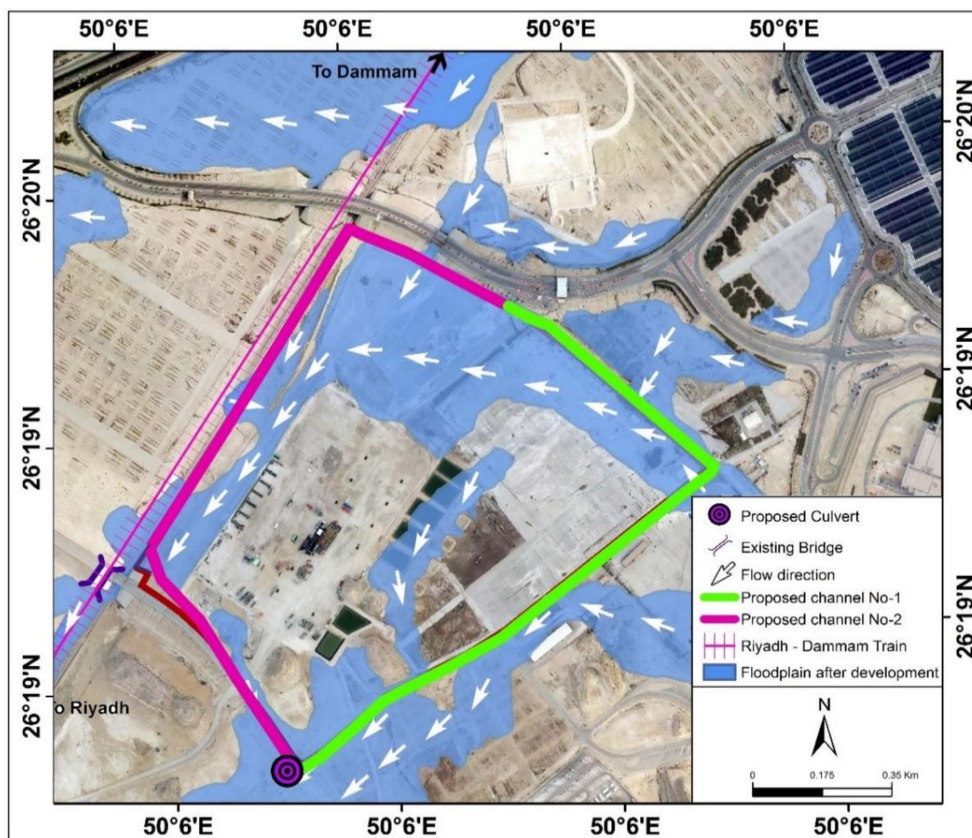


Figure 19. The first proposed scenario for the plan to protect the Riyadh–Dammam train track.

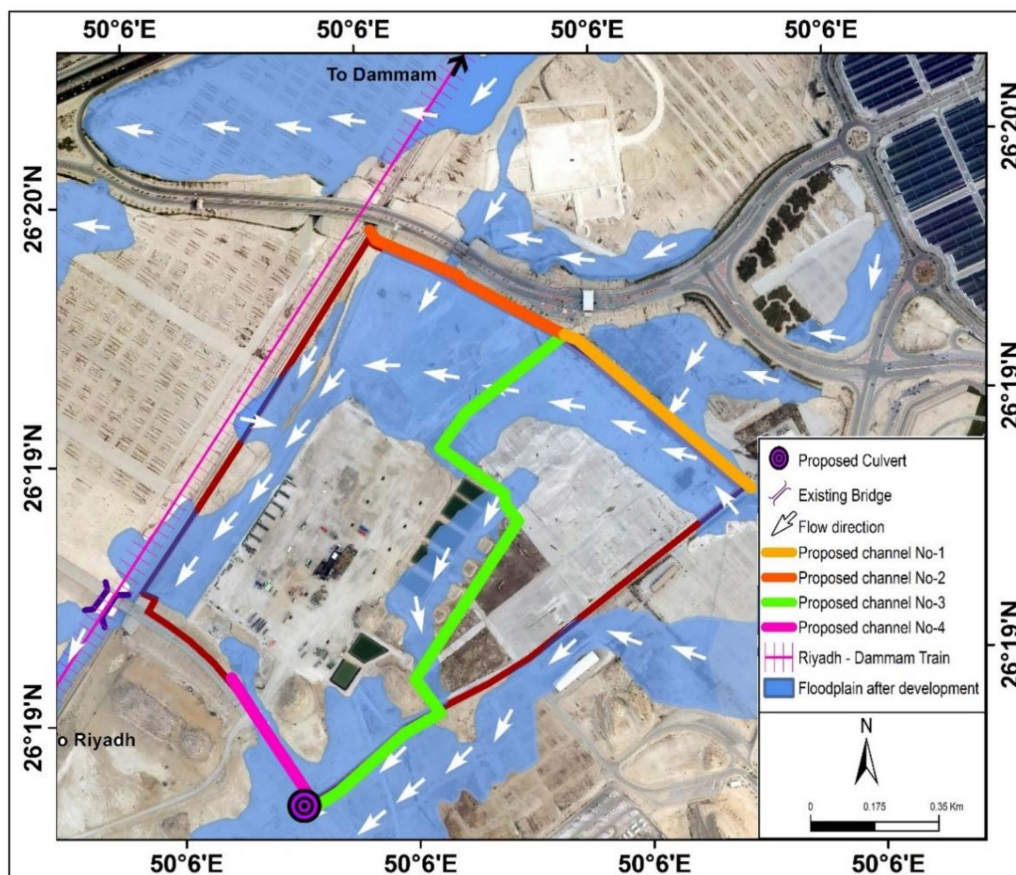


Figure 20. The second proposed scenario for the plan to protect the Riyadh–Dammam train track.

## 6. Conclusions

Sustainable development of the study area has been threatened by ignoring integrated maps of flood hazards, which represent historical changes in the land cover of the Riyadh–Dammam train crash area. The Riyadh–Dammam train track has been exposed to the risks of floods that have caused much damage to life, property, and infrastructure and have led to the flooding of nearby urban complexes.

This mainly is due to the limitations of unbalanced urban development, especially imposed interventions in changing the use of land for planning purposes. The study area witnessed changes in the use of land, the most prominent of which was the increase in the area of construction buildings by 292%, from 2.5 hectares in 2011 to 9.8 hectares in 2017. In 2017, the land-use map also saw the construction of seven storage basins, with an area of 1.5 hectares. The second thing was the increase in the height of the natural land levels in the center of the area almost as a result of the filling operations and the construction of a concrete layer in preparation for the construction of storage basins. Notably, the facilities that have been developed have raised the level of land in the middle part by at least 1 to 2 m.

The third matter is the morphology of the shape of the wadies between 2011 and 2017. In terms of the direction of the flow path, the intensity of discharge to the north instead of the south, and the presence of erosion to the south of the study site, there is evidence of geomorphological changes indicating the intensity of the discharge in the study area that is cut off by transit waterways.

The fourth matter is revealed by the results of the hydraulic analysis in 2017. The floodwaters did not interrupt or cross the railway track in 2011, but the situation changed after 2017 as the floodwaters interrupted the track in two locations. The first site had a depth of 1.86 m with a speed of 0.43 m/s. The second location was at the corner of the study area on the southwest side with a depth of 0.57 m and a speed of 4.91 m/s.

The fifth matter is that there are many existing hydraulic structures (ferries, bridges, and canals) that flow directly towards the train track. The study area has become a collection point for water coming from the southeast and northeast, which is extremely dangerous, and is coupled with the inability of drainage facilities to remove water. The existing flood waters of bridges located below the north train track pass peak flows to the wadies affecting them, resulting in significant damage to the train, property, and personnel.

There is no doubt that these major changes played a crucial role in the change of morphology of land use and was a clear point of objection in the way of wadies becoming a large part of the direction of flow. Flow is heading towards the northwest, i.e., towards the train track. This is possibly the real danger and is the main reason for the change of water flow from the Southern Side of Di' Al Midra Al Janubi wadi, which caused the Riyadh–Dammam train to drift on 18 February 2017 at kilo (10) in the west of Dhahran neighborhood.

Thus, this poses a schematic question: to what extent is the land use map and increased flood risk affected by political decisions taken by the Governmental Authorities over time and by the various development projects that they are implementing? The answer to this question is that managing the problems of urban expansion and land use change, as well as studying the prevention of flood hazards before the preparation of urban plans, have encountered some difficulties in the Kingdom, especially in a city like Dammam in which the disaster of train derailment took place. Knowledge, information, and management expertise in the city of Dammam has not been at the level at which they can be relied upon to address these problems. Moreover, dealing with the challenges of rapid, wide-ranging, inclusive, and varying dimensions and patterns of urban growth, and linking it to the risks of possible flood burdens, is necessary for any government or local administration, regardless of its longevity and experience. This study illustrates the risks of the continuation of urban expansion and land-use change in the valleys, which accelerates the need to pre-plan the cities that grow at the expense of the valleys in the dry areas. Thus, active flood valley routs should be identified, and infringements on them should be prevented. Therefore, the study presented a suggested mechanism to prevent the dangers of floods on the route of the Riyadh–Dammam train, which is suitable based on its spatial and urban nature. This mechanism should be adhered to in order to manage the urban environment in light of recurring flood incidents.

The present study will be an important criterion for planners and policymakers in Saudi Arabia as well as researchers in land-use change and flood risk prevention, as its vision and outputs can serve as key inputs for sustainable land use plans and strategies to mitigate flood risk. Moreover, the study represents an applied model for the management of the infrastructure against flood risks, and it is a critical approach to the assessment of flood risks of the infrastructure of railway tracks.

**Author Contributions:** A.A. designed the study, developed the research idea and planned the research activities. A.A., A.F.D.G., H.M.A. and I.I.A. carried out the research, including collecting the input data and preparing the manuscript, carried out a statistical analysis of the obtained results. A.A. carried out statistical and spatial analyses of two-dimensional Hydraulic modeling using HEC–RAS, replied to the reviewers' comments, wrote the manuscript, provided valuable comments in writing this paper, professionally edited the manuscript, and designed the methodology. I.I.A. carried out statistical and spatial analyses of monitoring the changes in land use. A.F.D.G. and H.M.A. carried out statistical and spatial analyses of monitoring the changes in morphology of the valleys in the study area.

**Funding:** This research was funded by the Deanship of Scientific Research at Princess Nourah bint Abdulrahman University through the Fast-track Research Funding Program.

**Acknowledgments:** The authors highly appreciate the great support from the Deanship of Scientific Research at Princess Nourah bint Abdulrahman University through the Fast-track Research Funding Program.

**Conflicts of Interest:** The authors declare no conflicts of interest.

## References

1. Istomina, M.N.; Kocharyan, A.G.; Lebedeva, I.P. Floods: Genesis, socioeconomic and environmental impacts. *Water Resour.* **2005**, *32*, 349–358. [[CrossRef](#)]

2. Brath, A.; Montanari, A.; Moretti, G. Assessing the effect on flood frequency of land use change via hydrological simulation (with uncertainty). *J. Hydrol.* **2006**, *324*, 141–153. [[CrossRef](#)]
3. Mao, D.; Cherkauer, A. Impacts of land-use change on hydrologic responses in the Great Lakes region. *J. Hydrol.* **2009**, *374*, 71–82. [[CrossRef](#)]
4. Sheng, J.; Wilson, J.P. Watershed urbanization and changing flood behavior across the Los Angeles metropolitan region. *Nat. Hazards* **2009**, *48*, 41–57. [[CrossRef](#)]
5. Solin, L.; Feranec, J.; Novacek, J. Land cover changes in small catchments in Slovakia during 1990–2006 and their effects on frequency of flood events. *Nat. Hazards* **2011**, *56*, 195–214. [[CrossRef](#)]
6. Rawat, S.; Biswas, V.; Kumar, M. Changes in land use/cover using geospatial techniques: A case study of Ramnagar town area, district Nainital, Uttarkhand, India. *Egypt J. Remote Sens. Space Sci.* **2013**, *16*, 111–117. [[CrossRef](#)]
7. Chaurasia, R.; Loshali, C.; Dhaliwal, S.; Sharma, K.; Kudrat, M.; Tiwari, K. Land use change analysis for agricultural management—A case study of Tehsil Talwandi Sabo, Punjab. *J. Indian Soc. Remote Sens.* **1996**, *24*, 115–123. [[CrossRef](#)]
8. Fernandez, S.; Lutz, A. Urban flood hazard zoning in Tucumán Province, Argentina, using GIS and multicriteria decision analysis. *Eng. Geol.* **2010**, *111*, 90–98. [[CrossRef](#)]
9. Abdel Karim, A.; Gaber, D.; Youssef, M.; Pradhan, B. Flood Hazard Assessment of the Urban Area of Tabuk City, Kingdom of Saudi Arabia by Integrating Spatial-Based Hydrologic and Hydrodynamic Modeling. *Sensors* **2019**, *19*, 1024. [[CrossRef](#)]
10. Nirupama, N.; Simonovic, S. Increase of flood risk because of urbanization: A Canadian example. *Nat. Hazards* **2007**, *40*, 25–41. [[CrossRef](#)]
11. Saghafian, B.; Farazjoo, H.; Bozorgy, B.; Yazdandoost, F. Flood intensification because of changes in land use. *Water Resour. Manag.* **2008**, *22*, 1051–1067. [[CrossRef](#)]
12. Suarez, P.; Anderson, W.; Mahal, V.; Lakshmanan, T.R. Impacts of flooding and climate change on urban transportation: A system wide performance assessment of the Boston Metro Area. *Transp. Res.* **2005**, *10*, 231–244. [[CrossRef](#)]
13. Ramachandra, V.; Mujumdar, P. Urban floods: Case study of Bangalore. *Disaster Dev.* **2009**, *3*, 1–98.
14. Huong, L.; Pathirana, A. Urbanization and climate change impacts on future urban flooding in Can Tho city, Vietnam. *Hydrol. Earth Syst. Sci.* **2013**, *17*, 379–394. [[CrossRef](#)]
15. Neuvel, M.; van den Brink, A. Flood risk management in Dutch local spatial planning practices. *J. Environ. Plan. Manag.* **2009**, *52*, 865–880. [[CrossRef](#)]
16. Audisio, C.; Turconi, L. Urban floods: A case study in the Savigliano area (North-Western Italy). *Nat. Hazards Earth Syst. Sci.* **2011**, *11*, 2951–2964. [[CrossRef](#)]
17. Špitalar, M.; Gourley, J.J.; Lutloff, C.; Kirstetter, P.E.; Brilly, M.; Carr, N. Analysis of flash flood parameters and human impacts in the US from 2006 to 2012. *J. Hydrol.* **2014**, *519*, 863–870. [[CrossRef](#)]
18. Ran, J.; Nedovic-Budic, Z. Integrating spatial planning and flood risk management: A new conceptual framework for the spatially integrated policy infrastructure. *Comput. Environ. Urban Syst.* **2016**, *57*, 68–79. [[CrossRef](#)]
19. Zhu, Z.; Woodcock, E. Continuous change detection and classification of land cover using all available Landsat data. *Remote Sens. Environ.* **2014**, *144*, 152–171. [[CrossRef](#)]
20. Seto, C.; Woodcock, E.; Song, C.; Huang, X.; Lu, J.; Kaufmann, K. Monitoring land-use change in the Pearl River Delta using Landsat TM. *Int. J. Remote Sens.* **2002**, *23*, 1985–2004. [[CrossRef](#)]
21. Ramachandra, V.; Kumar, U. Geographic Resources Decision Support System for land use/land cover dynamics analysis. In Proceedings of the FOSS/GRASS Users Conference, Bangkok, Thailand, 12–14 September 2004; Available online: <http://ces.iisc.ernet.in/energy/Welcome.html> (accessed on 4 May 2019).
22. Abdelsalam, G.; Youssef, M.; Arafat, M.; Alfarhan, M. The rise and demise of the new lakes of Sahara. *Geosphere* **2008**, *4*, 375–386. [[CrossRef](#)]
23. Im, J.; Jensen, J.; Tullis, J. Object-based change detection using correlation image analysis and image segmentation. *Int. J. Remote Sens.* **2008**, *29*, 399–423. [[CrossRef](#)]
24. Satir, O.; Berberoglu, S. Land use/cover classification techniques using optical remotely sensed data in landscape planning. In *Landscape Planning*; Özyavuz, R.M., Ed.; InTech: Horwich, UK, 2012; pp. 21–54. Available online: <https://www.intechopen.com/books/landscape-planning/land-use-cover-classification-techniques-using-optical-remotely-sensed-data-in-landscape-planning> (accessed on 16 April 2019).

25. Raziq, A.; Xu, A.; Li, Y.; Zhao, Q. Monitoring of land use/land cover changes and urban sprawl in Peshawar City in Khyber Pakhtunkhwa: An application of geo-information techniques using of multi-temporal satellite data. *J. Remote Sens.* **2016**, *5*, 174. Available online: <https://www.omicsonline.org/open-access/monitoring-of-land-useland-cover-changes-and-urban-sprawlin-peshawar-city-in-khyber-pakhtunkhwa-an-application-of-geoinformation-t-2469-4134-10001704.php?aid=82444> (accessed on 15 March 2019). [CrossRef]
26. Berberoglu, S.; Satir, O.; Atkinson, M. Mapping percentage tree cover from Envisat MERIS data using linear and non-linear techniques. *Int. J. Remote Sens.* **2009**, *30*, 4747–4766. [CrossRef]
27. Donmez, C.; Berberoglu, S.; Curran, P. Modelling the current and future spatial distribution of NPP in a Mediterranean watershed. *Int. J. Appl. Earth Obs. Geoinf.* **2011**, *13*, 336–345. [CrossRef]
28. Akin, A.; Sunar, F.; Berberoglu, S. Urban change analysis and future growth of Istanbul. *Environ. Monit. Assess.* **2015**, *187*, 506. [CrossRef]
29. Alqurashi, A.; Kumar, L.; Sinha, P. Urban land cover change modeling using time-series satellite images: A case study of urban growth in five cities of Saudi Arabia. *Remote Sens.* **2016**, *8*, 838. [CrossRef]
30. Liu, F.; Zhang, Z.; Wang, X. Forms of urban expansion of Chinese municipalities and provincial capitals, 1970s–2013. *Remote Sens.* **2016**, *8*, 930. [CrossRef]
31. Cao, H.; Liu, J.; Fu, C.; Zhang, W.; Wang, G.; Yang, G.; Luo, L. Urban expansion and its impact on the land use pattern in xishuangbanna since the reform and opening up of China. *Remote Sens.* **2017**, *9*, 137. [CrossRef]
32. Gumma, K.; Mohammad, I.; Nedumaran, S.; Whitbread, A.; Lagerkvist, J. Urban sprawl and adverse impacts on agricultural land: A case study on Hyderabad, India. *Remote Sens.* **2017**, *9*, 1136. [CrossRef]
33. Parece, E.; Campbell, B. Geospatial evaluation for urban agriculture land inventory: Roanoke, Virginia, USA. *Int. J. Appl. Geospat. Res.* **2017**, *8*, 43–63. Available online: <https://www.igi-global.com/gateway/article/169736> (accessed on 2 March 2019). [CrossRef]
34. Dawod, G.; Mohamed, W. Data management of different height systems within GPS/GIS integrated spatial technology. In Proceedings of the Middle East Spatial Technology Conference (MEST2009), Manama, Bahrain, 7–9 December 2009; pp. 1–15. Available online: [https://www.academia.edu/801459/DATA\\_MANAGEMENT\\_OF\\_DIFFERENT\\_HEIGHT\\_SYSTEMS\\_WITHIN\\_GPS\\_GIS\\_INTEGRATED\\_SPATIAL\\_TECHNOLOGY](https://www.academia.edu/801459/DATA_MANAGEMENT_OF_DIFFERENT_HEIGHT_SYSTEMS_WITHIN_GPS_GIS_INTEGRATED_SPATIAL_TECHNOLOGY) (accessed on 13 May 2019).
35. El-Bastawesy, M.; Faid, A.; El-Gammal, E. The Quaternary development of tributary channels to the Nile River at Kom Ombo area, Eastern Desert of Egypt, and their implication for groundwater resources. *J. Hydrol. Process.* **2010**, *24*, 1856–1865. [CrossRef]
36. Dawod, G.; Mohamed, H. Estimation of sea level rise hazardous impacts in egypt within a GIS environment. In Proceedings of the Third National GIS Symposium in Saudi Arabia, Al-Khobar City, Saudi Arabia, 7–9 April 2008; pp. 1–14. Available online: [https://www.academia.edu/794551/ESTIMATION\\_OF\\_SEA\\_LEVEL\\_RISE\\_HAZARDOUS\\_IMPACTS\\_IN\\_EGYPT\\_WITHIN\\_A\\_GIS\\_ENVIRONMENT](https://www.academia.edu/794551/ESTIMATION_OF_SEA_LEVEL_RISE_HAZARDOUS_IMPACTS_IN_EGYPT_WITHIN_A_GIS_ENVIRONMENT) (accessed on 4 June 2019).
37. Xu, C.; Chen, Y.; Chen, Y.; Zhao, R.; Ding, H. Responses of surface runoff to climate change and human activities in the arid region of Central Asia: A case study in the Tarim River Basin, China. *Environ. Manag.* **2013**, *51*, 926–938. [CrossRef] [PubMed]
38. Poussin, J.K.; Botzen, W.; Aerts, H. Factors of influence on flood damage mitigation behavior by households. *Environ. Sci. Policy* **2014**, *40*, 69–77. [CrossRef]
39. Patel, D.P.; Srivastava, K. Flood hazards mitigation analysis using remote sensing and GIS: Correspondence with town planning scheme. *Water Resour. Manag.* **2013**, *27*, 2353–2368. [CrossRef]
40. Moel, D.; Vliet, V.; Aerts, H. Evaluating the effect of flood damage-reducing measures: A case study of the unembanked area of Rotterdam, The Netherlands. *Reg. Environ. Change* **2014**, *14*, 895–908. [CrossRef]
41. Althuwaynee, F.; Pradhan, B.; Park, J.; Lee, H. A novel ensemble bivariate statistical evidential belief function with knowledge-based analytical hierarchy process and multivariate statistical logistic regression for landslide susceptibility mapping. *Catena* **2014**, *114*, 21–36. [CrossRef]
42. Van, J.; Rengers, N.; Soeters, R. Use of geomorphological information in indirect landslide susceptibility assessment. *Nat. Hazards* **2003**, *30*, 399–419. [CrossRef]
43. Lee, J.; Kang, E.; Jeon, S. Application of frequency ratio model and validation for predictive flooded area susceptibility mapping using GIS. In Proceedings of the Geoscience and Remote Sensing Symposium (IGARSS), Munich, Germany, 22–27 July 2012; pp. 895–898. [CrossRef]

44. Tehrany, S.; Pradhan, B.; Mansor, S.; Ahmad, N. Flood susceptibility assessment using GIS-based support vector machine model with different kernel types. *Catena* **2015**, *125*, 91–101. [[CrossRef](#)]
45. Stefanidis, S.; Stathis, D. Assessment of flood hazard based on natural and anthropogenic factors using analytic hierarchy process (AHP). *Nat. Hazards* **2013**, *68*, 569–585. [[CrossRef](#)]
46. Pradhan, B. Use of GIS-based fuzzy logic relations and its cross application to produce landslide susceptibility maps in three test areas in Malaysia. *Environ. Earth Sci.* **2011**, *63*, 329–349. [[CrossRef](#)]
47. Pradhan, B. Flood susceptible mapping and risk area delineation using logistic regression, GIS and remote sensing. *J. Spat. Hydrol.* **2010**, *9*, 1–18.
48. Samanta, S.; Pal, K.; Lohar, D.; Pal, B. Interpolation of climate variables and temperature modeling. *Theor. Appl. Clim.* **2012**, *107*, 35–45. [[CrossRef](#)]
49. Kia, B.; Pirasteh, S.; Pradhan, B.; Rodzi, A.; Sulaiman, A.; Moradi, A. An artificial neural network model for flood simulation using GIS: Johor River Basin, Malaysia. *Environ. Earth Sci.* **2012**, *67*, 251–264. [[CrossRef](#)]
50. Lohani, K.; Goel, K.; Bhatia, S. Improving real time flood forecasting using fuzzy inference system. *J. Hydrol.* **2014**, *509*, 25–41. [[CrossRef](#)]
51. Tehrany, S.; Pradhan, B.; Jebur, N. Flood susceptibility mapping using a novel ensemble weights-of-evidence and support vector machine models in GIS. *J. Hydrol.* **2014**, *512*, 332–343. [[CrossRef](#)]
52. Koloa, C.; Samanta, S. Development Impact Assessment Along Merkhram River through Remote Sensing and GIS Technology. *Int. J. Asian Acad. Res. Assoc.* **2013**, *5*, 26–41.
53. Malczewski, J. GIS-based multicriteria decision analysis: A survey of the literature. *Int. J. Geogr. Inf. Sci.* **2006**, *20*, 703–726. [[CrossRef](#)]
54. Jia, Y.; Wang, S. *CCHE2D: Two-Dimensional Hydrodynamic and Sediment. Transport. Model. for Unsteady Open Channel Flows Over Loose Bed*; National Center of Computational Hydroscience and Engineering: Nutrioso, AZ, USA, 2001.
55. O'Brien, S. FLO-2D: Two-Dimensional Flood Routing Mode; FLO-2D Software. 2017. Available online: [www.flo-2d.com/wp-content/uploads/2018/09/FLO-2D-Plugin-Users-Manual.pdf](http://www.flo-2d.com/wp-content/uploads/2018/09/FLO-2D-Plugin-Users-Manual.pdf) (accessed on 12 November 2018).
56. Deltares. *SOBEK: Hydrodynamics, Rainfall and Real-Time Control. User Manual*; Deltares: Delft, The Netherlands, 2019; pp. 1–932. Available online: <http://www.deltares.nl> (accessed on 16 November 2018).
57. Danish Hydraulic Institute. *MIKE-Flood User Manual*; Danish Hydraulic Institute: Horsholm, Denmark, 2017; pp. 1–152.
58. Bradbrook, K. JFLOW: A multiscale two-dimensional dynamic flood model. *J. Water Environ. Technol.* **2007**, *2*, 79–86. [[CrossRef](#)]
59. Bates, P.; Trigg, M.; Neal, J.; Dabrowa, A. *LISFLOOD-FP User Manual*; University of Bristol: Bristol, UK, 2013.
60. Khabat, K.; Himan, S.; Binh, T.; Jan, A.; Ataollah, S.; Biswajeet, P.; Jie, D.; Hai-Bang, L.; Gyula, G.; Huu, L.; et al. A comparative assessment of flood susceptibility modeling using multi-criteria decision-making analysis and machine learning methods. *J. Hydrol.* **2019**, *573*, 311–323. [[CrossRef](#)]
61. Wang, Y.; Hong, H.; Chen, W.; Li, S.; Pamučar, D.; Gigović, L.; Drobnjak, S.; Tien Bui, D.; Duan, H. A Hybrid GIS multi-criteria decision-making method for flood susceptibility mapping at Shangyou, China. *Remote Sens.* **2019**, *11*, 62. [[CrossRef](#)]
62. Shivaprasad, S.; Parth, S.; Chakravarthi, V.; Srinivasa, R. Flood risk assessment using multi-criteria analysis: A case study from Kopili River Basin, Assam, India. *Geomat. Nat. Hazards Risk* **2018**, *9*, 79–93. [[CrossRef](#)]
63. Sailesh, S.; Dilip, K.; Babita, P. Flood susceptibility analysis through remote sensing, GIS and frequency ratio model. *Appl. Water Sci.* **2018**, *8*, 66. [[CrossRef](#)]
64. Khabat, K.; Ebrahim, N.; Edris, M.; Hamid, R. A GIS-based flood susceptibility assessment and its mapping in Iran: A comparison between frequency ratio and weights-of-evidence bivariate statistical models with multi-criteria decision-making technique. *J. Nat. Hazards* **2016**, *83*, 947–987. [[CrossRef](#)]
65. Getahun, Y.; Gebre, S. Flood hazard assessment and mapping of flood inundation area of the awash river basin in ethiopia using GIS and HECGeoRAS /HEC-RAS model. *J. Civil. Environ. Eng.* **2015**, *5*, 1–12. [[CrossRef](#)]
66. Olga, P.; Nerantzis, K.; Ioannis, K.; Thomas, P.; Nicolaos, T.; Konstantinos, V. Assessing flood hazard at river basin scale with an index-based approach: The case of Mouriki, Greece. *Geosciences* **2018**, *8*, 50. [[CrossRef](#)]
67. Clement, K.; Edward, M. Accra flood modelling through application of geographic information systems (GIS), remote sensing techniques and analytical hierarchy process. *J. Remote Sens. GIS* **2017**, *191*, 6. [[CrossRef](#)]

68. Martin, K.; Joshua, E.; Hongtao, W.; Fengting, L. Characterizing flood hazard risk in data-scarce areas, using a remote sensing and GIS-based flood hazard index. *Nat. Hazards* **2017**, *89*, 1369. [[CrossRef](#)]
69. Doocy, S.; Daniels, A.; Murray, S.; Kirsch, T.D. The human impact of floods: A historical review of events 1980–2009 and systematic literature review. *PLoS Curr.* **2017**, *5*, 1–19. [[CrossRef](#)]
70. US Army Corps of Engineers (USACE). *Hydrologic Modeling System HEC-HMS Technical Reference Manual*; Hydrologic Engineering Center: Davis, CA, USA, 2000.
71. Soil Conservation Services, (SCS). *National Engineering Handbook. Section 4: Hydrology*; US Department of Agriculture, Soil Conservation Service, Engineering Division: Washington, DC, USA, 1985.
72. Hyfran, M. Developed by INRS-Eau with Collaboration of Hydro-Québec Hydraulic Service (Department Hydrology) in the Framework of Hydro-Québec/CRSNG Statistical Hydrology Chair Located at INRS-Eau. 1998. Available online: <http://www.wrpllc.com/books/hyfran.html> (accessed on 10 May 2019).
73. Ponce, V.M.; Hawkins, R.H. Runoff Curve Number: Has It Reached Maturity? *J. Hyrol. Eng.* **1996**, *1*, 9–20. [[CrossRef](#)]
74. Blöschl, G.; Nester, T.; Komma, J.; Parajka, J.; Perdigão, P. The June 2013 flood in the Upper Danube Basin, and comparisons with the 2002, 1954 and 1899 floods. *Hydrol. Earth Syst. Sci.* **2013**, *17*, 5197–5212. [[CrossRef](#)]
75. Faccini, F.; Paliaga, G.; Piana, P.; Sacchini, A.; Watkins, C. The Bisagno stream catchment (Genoa, Italy) and its major floods (1822, 1970 and 2014): Geomorphic and land use variations in the last three centuries. *Geomorphology* **2016**, *273*, 14–27. [[CrossRef](#)]
76. Paliaga, G.; Faccini, F.; Luino, F.; Turconi, L. A spatial multicriteria prioritizing approach for geohydrological risk mitigation planning in small and densely urbanized Mediterranean basins. *Nat. Hazards Earth Syst. Sci.* **2019**, *19*, 53–69. [[CrossRef](#)]
77. Piana, P.; Faccini, F.; Luino, F.; Paliaga, G.; Sacchini, A.; Watkins, C. Geomorphological landscape research and flood management in a heavily modified Tyrrhenian catchment. *Sustainability* **2019**, *11*, 4594. [[CrossRef](#)]



© 2019 by the authors. Licensee MDPI, Basel, Switzerland. This article is an open access article distributed under the terms and conditions of the Creative Commons Attribution (CC BY) license (<http://creativecommons.org/licenses/by/4.0/>).